

NASA TECHNICAL NOTE



NASA TN D-2163

C 1

LOAN COPY NO. 1000
AFWL (AFW-2) TO
KIRTLAND AFB, N M



NASA TN D-2163

AERODYNAMIC CHARACTERISTICS FROM
MACH 0.22 TO 4.65 OF A TWO-STAGE ROCKET
VEHICLE HAVING AN UNUSUAL NOSE SHAPE

by John T. Suttles

Langley Research Center

Langley Station, Hampton, Va.

NATIONAL AERONAUTICS AND SPACE ADMINISTRATION • WASHINGTON, D. C. • NOVEMBER 1964

TECH LIBRARY KAFB, NM



0154353

AERODYNAMIC CHARACTERISTICS FROM MACH 0.22 TO 4.65 OF A
TWO-STAGE ROCKET VEHICLE HAVING AN UNUSUAL NOSE SHAPE

By John T. Suttles

Langley Research Center
Langley Station, Hampton, Va.

NATIONAL AERONAUTICS AND SPACE ADMINISTRATION

For sale by the Office of Technical Services, Department of Commerce,
Washington, D.C. 20230 -- Price \$1.50

AERODYNAMIC CHARACTERISTICS FROM MACH 0.22 TO 4.65 OF A
TWO-STAGE ROCKET VEHICLE HAVING AN UNUSUAL NOSE SHAPE

By John T. Suttles
Langley Research Center

SUMMARY

An investigation has been conducted in various wind-tunnel facilities at the Langley Research Center to determine the aerodynamic characteristics of a two-stage rocket vehicle having an unusual nose shape. This unusual nose consists of a blunted cone followed by a square body segment which terminates in a conical flare. Four fairings are located near the conical nose and on the flat surfaces of the square body segment. The tests were conducted for subsonic, transonic, and supersonic Mach numbers. The angle of attack was varied from about -2° to 95° for the subsonic tests and the angles of attack and sideslip were varied from about -8° to 8° for the transonic and supersonic tests.

Results are presented showing the variation of the aerodynamic forces, moments, and centers of pressure with Mach number, angle of attack, and angle of sideslip. The effects of two auxiliary rocket motors attached to the first stage were investigated at subsonic, transonic, and supersonic speeds. They were found to cause very small changes in stability level but increased the axial force by up to 16 percent. The effects of the four fairings at the nose were investigated at supersonic speeds. The fairings were found to produce a small decrease in the stability level and an increase in drag of up to 13 percent. Data for the configuration without auxiliary rockets and fins were obtained at supersonic speeds so that the fin and body contributions to the aerodynamics could be determined. The results of a comparison of estimated and measured fin and body aerodynamic characteristics indicated that reasonable estimates could be made of the effect of the fins on the static stability and axial-force characteristics. By assuming a simplified shape for the body, reasonable estimates were made for the body contribution to the static stability; however, this assumption led to estimates of the axial force which were considerably lower than the measured values.

INTRODUCTION

The National Aeronautics and Space Administration has undertaken a general program to evaluate various rocket-vehicle control-system concepts. One such control system in conjunction with a two-stage rocket vehicle has been described in reference 1. The vehicle consists of two stages with a spacecraft compartment mounted at the forward end of the second stage. Housed within this spacecraft

compartment is the control system which is used to stabilize and control the second stage. The second stage with its spacecraft compartment is placed in a near space environment by the fin-stabilized first stage which does not utilize a control system. A prerequisite to the study of the dynamics of such a rocket vehicle is the determination of the aerodynamic characteristics of the configuration.

The configuration of the spacecraft compartment of the vehicle described in reference 1 has an unusual shape because of the requirements for housing the particular control system used. This shape consists of a blunted, conical nose followed by the main body of the spacecraft which has a square cross section. On each of the flat surfaces of this section is a fairing which is used to protect vulnerable portions of the control system during atmospheric flight. Because of the design of the control system, the fairings are asymmetrically located. The square section then joins a conical flare which terminates in the cylindrical diameter of the second stage. This configuration is very unusual and an analytical analysis of the aerodynamic effects of the shape would be difficult if not impossible to obtain.

Wind-tunnel tests were therefore conducted at the Langley Research Center to determine the aerodynamic characteristics of the two-stage research rocket vehicle described in reference 1. These data are needed for use in simulations of the dynamics of the vehicle and for determining structural loads. For vehicles such as that being considered, three specific problem areas require the use of accurate aerodynamic data. Subsonic high-angle-of-attack data are necessary for use in a wind-compensation procedure prior to launch. This procedure is required since the vehicle being studied does not utilize a control system during the exit or first-stage boost phase. Transonic force and moment data are necessary since the maximum aerodynamic loading most often occurs in this speed range. The static stability of fin-stabilized rocket vehicles often is a minimum at high supersonic speeds. Supersonic data are therefore required to be sure that the vehicle being studied possesses sufficient static stability for the uncontrolled portion of the flight.

The data presented herein are results of tests of a 0.10-scale model of the vehicle at subsonic, transonic, and supersonic Mach numbers. For the subsonic tests the angle of attack was varied from approximately -2° to 95° at zero angle of sideslip. The transonic and supersonic tests were conducted for angles of attack and sideslip from about -8° to 8° . Aerodynamic forces, moments, and centers of pressure were determined for the basic vehicle configuration. The effect on the vehicle aerodynamics of two auxiliary booster rockets attached to the first stage was investigated for subsonic, transonic, and supersonic Mach numbers. The effect of the four fairings near the nose was investigated at supersonic speeds. Data for the basic configuration without auxiliary rockets and fins were obtained at supersonic speeds so that the fin and body contributions to the aerodynamics could be determined. Estimates were made of the effect on the aerodynamic characteristics of the fins and the body. In order to make these estimates, a simplified body shape was assumed. These data are compared with the measured fin and body contributions.

SYMBOLS

The coefficients of forces and moments are referred to the body-axis system. (See fig. 1.) Aerodynamic moments presented are referenced to a moment center located 21.60 inches back of the model theoretical nose apex as shown in figure 2. Coefficients are based on the first-stage body diameter of 3.10 inches and a corresponding area of 0.0524 square foot.

C_A	axial-force coefficient, $\frac{\text{Axial force}}{qS}$
$C_{A,0}$	axial-force coefficient at an angle of attack of 0°
C_l	rolling-moment coefficient, $\frac{\text{Rolling moment}}{qSd}$
C_m	pitching-moment coefficient, $\frac{\text{Pitching moment}}{qSd}$
$C_{m\alpha}$	slope of pitching-moment curve through an angle of attack of 0°
C_N	normal-force coefficient, $\frac{\text{Normal force}}{qS}$
$C_{N\alpha}$	slope of normal-force curve through an angle of attack of 0°
C_n	yawing-moment coefficient, $\frac{\text{Yawing moment}}{qSd}$
$C_{n\beta}$	slope of yawing-moment curve through an angle of sideslip of 0°
C_y	side-force coefficient, $\frac{\text{Side force}}{qS}$
$C_{y\beta}$	slope of side-force curve through an angle of sideslip of 0°
d	diameter of first stage of test configuration, in.
M	free-stream Mach number
q	free-stream dynamic pressure, lb/sq ft
R	radius of nose, in.
S	cross-sectional area of first stage of test configuration, sq ft

$$\left(\frac{x_{cp}}{d}\right)_\alpha$$

center-of-pressure location in pitch plane, body diameters forward of model base

$$\left(\frac{x_{cp}}{d}\right)_\beta$$

center-of-pressure location in yaw plane, body diameters forward of model base

$$\frac{x_{mc}}{d}$$

location of balance center, body diameters forward of model base

α

angle of attack of model center line, deg

β

angle of sideslip of model center line, deg

• Δ

incremental change due to presence of fairings or auxiliary rockets

APPARATUS AND TESTS

Model

Model details and dimensions are presented in the drawings shown in figure 2 and in the photographs of figure 3. The model is a 0.10-scale model of the research vehicle described in reference 1. The basic configuration consists of a first stage composed of a fin-stabilized booster with two auxiliary rockets to give additional take-off acceleration and a second stage composed of a rocket motor with a spacecraft compartment mounted on its forward end. A control system is housed in this compartment and is used to maintain stability and provide control for the second stage after separation from the uncontrolled first-stage booster.

The first stage is equipped with a cruciform arrangement of modified double-wedge fin panels, one of which is shown in detail in figure 2(b). The fin panels had an aspect ratio of 1.5, a leading-edge sweep of $18^{\circ}24'$ and represented full-scale panels of 12 square feet. The model was mounted in the tunnel so that the planes formed by the fin panels made an angle of 45° with the pitch and yaw axes. The first-stage auxiliary rocket motors, shown mounted on the vehicle in figure 2(a), are shown in detail in figure 2(b). The control rocket fairings on the spacecraft compartment, shown on the model in figure 2(a), are used to protect the exposed ends of the control rockets through the period of high aerodynamic heating and dynamic pressure encountered during ascent. Details of the fairings and the protruding ends of the control rockets are illustrated in figure 2(c). The model tested was constructed so that the configuration with and without the fairings, fins, and auxiliary rockets could be simulated. Other features simulated on the model such as the wiring tunnels and separation band are illustrated in figure 2(a) and may be seen in the photographs of figure 3.

Tests and Procedure

Subsonic tests.- The subsonic tests were conducted in the Langley 300-MPH 7- by 10-foot tunnel at a Mach number of 0.22. The Reynolds number per foot was maintained at 1.53×10^6 and the angle of attack was varied from -20° to 95° at zero angle of sideslip. Results for these tests are presented for the basic configuration, the basic configuration at a 45° roll angle, and the basic configuration with the auxiliary rockets removed. With the model rolled 45° (clockwise when viewed from rear), the fin panels were alined with the pitch and yaw axes and the auxiliary rockets lay in a plane making a 45° angle with the pitch and yaw axes.

Transonic tests.- The transonic tests were conducted in the Langley 8-foot transonic pressure tunnel for Mach numbers of 0.60, 0.80, 0.90, 0.95, and 1.03. The angle of attack was varied from approximately -8° to 8° at zero angle of sideslip and the angle of sideslip was varied from about -8° to 8° at zero angle of attack. The Reynolds number per foot was maintained at approximately 1.35×10^6 for these tests. Two model configurations were tested, the basic configuration and the basic configuration with the auxiliary rockets removed. Because of the low Reynolds number these tests were conducted with a transition strip located 1.50 inches from the nose-cone theoretical apex. A strip 0.10 inch wide and composed of no. 60 carborundum grains set in a plastic adhesive was used.

Supersonic tests.- The supersonic tests were conducted in the high-speed section of the Langley Unitary Plan wind tunnel. The basic configuration, the basic configuration with auxiliary rockets removed, and the basic configuration with control rocket fairings removed were tested at Mach numbers of 2.30, 2.96, 3.96, and 4.65. In addition, the body alone (basic configuration with auxiliary rockets and fins removed) was tested at these Mach numbers. During all tests the Reynolds number per foot was maintained at about 2.8×10^6 and the angle of attack was varied from approximately -8° to 8° at zero angle of sideslip and the angle of sideslip was varied from about -8° to 8° at zero angle of attack.

Measurements

In all tests reported herein, aerodynamic forces and moments were determined by means of a six-component electrical strain-gage balance housed within the body of the model. The balance, in turn, was rigidly fastened to a sting support. Because of balance component malfunctions, data were not obtained from the side-force component at some negative sideslip angles at transonic speeds and from the normal-force and pitching-moment components at some of the larger negative angles of attack at supersonic speeds.

Corrections

The data presented herein for all tests have been adjusted to correspond to the condition of free-stream static pressure acting at the model base and in the balance chamber.

For the subsonic and transonic tests, the effects of subsonic boundary interference in the test section were considered negligible and no corrections for this effect have been applied. For the transonic tests, data are not presented for Mach numbers at which supersonic boundary-reflected disturbances would be expected to affect the results. For this reason data in the transonic speed range are not presented at Mach numbers above 1.03. However, schlieren photographs of the flow over the nose are presented for Mach numbers up to 1.20.

In the transonic and supersonic tests, angles of attack were corrected for average tunnel flow angularity and for the deflection of the model and sting support as a result of aerodynamic loads.

It will be noted that the normal forces and pitching moments and the side forces and yawing moments do not pass through zero at zero angles of attack and sideslip, respectively. This result indicates that there was a model misalignment or error in determining the effective angles of attack and sideslip since the effective aerodynamic shape is symmetrical in the pitch and yaw planes. These characteristics were not corrected for the bias in the data; however, the slopes or aerodynamic derivatives discussed herein are not affected. The center-of-pressure data are affected and special care was taken in computing these data so as not to present erroneous variations with angle of attack and sideslip. These calculations were made for the pitch data by cross plotting the normal force against the pitching moment at angles of attack. A curve was faired through the data and this curve was shifted so that it passed through the origin. The centers of pressure were then computed for points on this curve and plotted against the corresponding angle of attack. The centers of pressure were computed from the following equation:

$$\left(\frac{x_{cp}}{d} \right)_{\alpha} = \frac{C_m}{C_N} + \frac{x_{mc}}{d} \quad (1)$$

Calculations were made for the yaw data in the same manner by using the following equation:

$$\left(\frac{x_{cp}}{d} \right)_{\beta} = \frac{C_n}{C_Y} + \frac{x_{mc}}{d} \quad (2)$$

Since data from faired curves were used in these computations, symbols are not used when presenting the center-of-pressure data.

Accuracy

The estimated accuracies of the measured coefficients, based on instrument calibration and data repeatability, are within the following limits:

Subsonic:

C_N	• •	$M = 0.22$	± 0.2
C_m	• • • • • • • • • • • • • • • • • • • •		± 0.2
C_A	• • • • • • • • • • • • • • • • • • •		± 0.02
C_l	• • • • • • • • • • • • • • • • • •		± 0.05

Transonic:

		$M = 0.60$	$M = 1.03$
C_N	• • • • • • • • • • • • • • • • • •	± 0.2	± 0.14
C_m	• • • • • • • • • • • • • • • • •	± 0.11	± 0.07
C_Y	• • • • • • • • • • • • • • • • •	± 0.19	± 0.1
C_n	• • • • • • • • • • • • • • • • •	± 0.19	± 0.1
C_A	• • • • • • • • • • • • • • • •	± 0.014	± 0.009
C_l	• • • • • • • • • • • • • • •	± 0.09	± 0.05

Supersonic:

		$M = 2.3$	$M = 4.65$
C_N	• • • • • • • • • • • • • • • • •	± 0.03	± 0.06
C_m	• • • • • • • • • • • • • • • •	± 0.02	± 0.04
C_Y	• • • • • • • • • • • • • • • •	± 0.03	± 0.06
C_n	• • • • • • • • • • • • • • •	± 0.02	± 0.04
C_A	• • • • • • • • • • • • • •	± 0.0075	± 0.015
C_l	• • • • • • • • • • • •	± 0.005	± 0.01

The limits for the subsonic coefficients ($M = 0.22$) apply to the low-angle-of-attack range ($\pm 15^\circ$). Accuracies at higher angles are not definite and therefore these data should be used to establish trends only. Model angle of attack and angle of sideslip are estimated to be accurate with $\pm 0.1^\circ$.

PRESENTATION OF RESULTS

The results presented in this report are for a vehicle which has an unusual nose configuration. This fact should be kept in mind in drawing conclusions from the results or in comparing the results with data for similar configurations. In order to facilitate presentation of the data, staggered scales have been used in some of the figures and care should be taken in selecting the proper zero axis for each curve. The figures presenting the results of this investigation are as follows:

Subsonic aerodynamic characteristics at angles of attack	Figure 4
Transonic aerodynamic characteristics at angles of attack and sideslip	5

Figure

Supersonic aerodynamic characteristics at angles of attack and sideslip	6
Effect of Mach number and configuration on zero angle-of-attack and angle-of-sideslip aerodynamic characteristics	7
Effect of configuration asymmetries on the Mach number variation of the zero angle-of-attack and angle-of-sideslip aerodynamic characteristics	8
Comparison of the estimated and measured aerodynamics for the fins and body illustrating the effect of the unusual nose shape	9

DISCUSSION OF RESULTS

Subsonic Data

The subsonic data are presented in figure 4. Data for all the configurations tested indicate that C_N and C_m vary linearly with angle of attack up to about 15° with significant nonlinear effects occurring at the higher angles. For the angle range in which C_N and C_m vary linearly with angle of attack, $\left(\frac{x_{cp}}{d}\right)_\alpha$ does not vary. At the high angles of attack $\left(\frac{x_{cp}}{d}\right)_\alpha$ shifts forward by a significant amount. The general trend in C_A variation is a decrease as the angle of attack is increased. The small values of C_l measured near zero angle of attack are close to the accuracy limit of these data. The spikes occurring in the C_l data at high angles are not reliable data. (See section entitled "Accuracy.")

The effects of the auxiliary rockets on the subsonic data are very small except at high angles of attack. At the high angles the auxiliary rockets increase the magnitude of C_N and C_m and cause a rearward shift in $\left(\frac{x_{cp}}{d}\right)_\alpha$ so that the stability is increased. They cause a small increase in C_A at the low angles of attack.

The effects of rolling the basic configuration 45° are also small at low angles of attack. At the high angles the magnitude of C_m is reduced and $\left(\frac{x_{cp}}{d}\right)_\alpha$ is shifted forward so that the static stability is reduced. In addition, there are significant values of C_l at the high angles which are probably due to the asymmetry created by the auxiliary rockets at this roll angle.

Transonic Data

The basic transonic data are presented in figures 5(a) to 5(h). Schlieren photographs of the flow field over the nose section at transonic Mach numbers are presented in figure 5(i). The range of angles of attack over which C_N and C_m vary linearly, approximately $\pm 4^\circ$, is smaller than that for the subsonic data. The presence of the auxiliary rockets does not significantly affect the linearity of C_N and C_m . As mentioned in the section on "Corrections," the bias in the data is not important; it is the slope of these curves which is of significance. The computed values of $\left(\frac{x_{cp}}{d}\right)_\alpha$ are constant in the range of angles where C_N and C_m vary linearly. In the range of nonlinear variations of C_N and C_m , there is a trend toward a forward shift in $\left(\frac{x_{cp}}{d}\right)_\alpha$. The variation of C_A with angle of attack in general is smooth with a decrease in C_A as the angle is increased from zero. A notable exception is the erratic variations at a Mach number of 0.95 for both the basic configuration and this configuration with the auxiliary rockets removed. This condition is probably caused by an unsteady flow field at the unusually shaped nose. The schlieren photographs of figure 5(i) show the changing shock-wave patterns on the nose at these Mach numbers. The effect of the auxiliary rockets is to increase C_A and angle-of-attack variations seem to have little effect on this axial-force increment. The rolling moments measured were very small and could have been caused by a slight misalignment of the first-stage fins. Such an effect will be shown in the discussion of the supersonic data. The directional static stability characteristics C_y , C_n , and $\left(\frac{x_{cp}}{d}\right)_\beta$ show the same characteristic variations with angle of sideslip as the longitudinal data show with angle of attack.

Supersonic Data

The basic supersonic data are presented in figures 6(a) to 6(j). Schlieren photographs of the flow over the entire vehicle at supersonic speeds are shown in figure 6(k). The variations of C_N and C_m with angle of attack are linear through a range of about $\pm 2^\circ$ only. The effects of the auxiliary rockets and control rocket fairings are small at low angles of attack. The data at the higher angles, however, do indicate that the auxiliary rockets measurably increase the magnitude of C_N and C_m and the fairings decrease the magnitude of C_m . The computed values of $\left(\frac{x_{cp}}{d}\right)_\alpha$ are constant at low angles with forward shifts in $\left(\frac{x_{cp}}{d}\right)_\alpha$ at the higher angles of attack.

The body alone, that is, the basic configuration with both the fins and auxiliary rockets removed, was also tested at supersonic speeds. (See fig. 6(d).) The variations of C_N and C_m with angle of attack for the body-alone configuration has a small linearity range of only $\pm 1^\circ$ or less. The relatively large variations of $\left(\frac{x_{cp}}{d}\right)_\alpha$ with angle of attack for the body-alone configuration is further indication of the nonlinear character of these data.

There were no significant variations of C_A with angle of attack for the configurations tested at supersonic speeds. The small values of C_l for the configurations with fins and the disappearance of these moments for the body-alone configuration is evidence of a small misalignment of the fins on the model.

The directional stability data $\left(C_Y, C_n, \text{ and } \left(\frac{x_{cp}}{d}\right)_\beta\right)$ have the same characteristic variations with angle of sideslip as did the longitudinal data with angle of attack.

Effect of Mach Number on Zero Angle of Attack

and Sideslip Characteristics

Presented in figures 7(a) to 7(g) are the aerodynamic derivatives, centers of pressure, and axial-force coefficients at zero angle of attack or sideslip for the test Mach number range. These data are shown for the basic configuration, the basic configuration with the auxiliary rockets removed, the basic configuration with the control rocket fairings removed, and for the basic configuration with the fins and auxiliary rockets removed. The results indicate that the auxiliary rockets have only small effects (less than 10 percent) on C_{N_α} ,

C_{m_α} , and $\left(\frac{x_{cp}}{d}\right)_{\alpha=0}$. This small effect, however, does indicate that the auxiliary rockets decrease the fin effectiveness at subsonic and transonic Mach numbers (positive ΔC_{m_α}). However, at the high supersonic Mach numbers the auxiliary rockets increase the fin effectiveness. The auxiliary rockets had a negligible effect (5 percent or less) on the directional stability characteristics $\left(C_{Y_\beta}, C_{n_\beta}, \text{ and } \left(\frac{x_{cp}}{d}\right)_{\beta=0}\right)$.

The auxiliary rockets increased $C_{A,0}$ by between 12 and 16 percent except in the drag-rise region where the increase was about 6 percent. The incremental effects due to the presence of the auxiliary rockets are presented in figure 7(h) for the longitudinal stability and axial-force characteristics and in figure 7(i) for the directional stability characteristics.

The effects of the control rocket fairings were only investigated at supersonic Mach numbers. The presence of the fairings was found to cause a definite decrease in the static longitudinal and directional stability levels (positive $\Delta C_{M\alpha}$ and negative $\Delta C_{n\beta}$, respectively). The changes in stability levels were associated with very small changes in $C_{N\alpha}$ and $C_{Y\beta}$ but definite forward shifts

in $\left(\frac{x_{cp}}{d}\right)_{\alpha=0}$ and $\left(\frac{x_{cp}}{d}\right)_{\beta=0}$. The presence of the control rocket fairings caused an increase in $C_{A,0}$ of about 6 percent at the lowest and about 13 percent at the highest supersonic Mach number.

The beneficial stability effects of the fins and the associated drag penalty may also be obtained from the data in figures 7(a) to 7(g). The fin effects are determined by comparing the configuration without auxiliary rockets with the configuration without auxiliary rockets and fins (body alone). These data are used in a subsequent figure to compare estimated fin and body contributions with the measured effects at supersonic Mach numbers.

Effect of Configuration Asymmetries on Zero Angle of Attack and Sideslip Characteristics

Since the control rocket fairings on the sides are forward of those on the top and bottom, there is an aerodynamic asymmetry between the longitudinal and directional stability planes. This asymmetry, however, is insignificant compared with the asymmetry arising from the fact that the two auxiliary rockets are fastened to the sides of the first stage. (See fig. 2(a).) With the auxiliary rockets located in this manner they increase the planform area of the basic configuration with respect to the longitudinal stability but create no change in the planform area affecting the directional stability. In order to investigate this asymmetry, the longitudinal and directional stability data for the basic configuration are compared in figure 8. Also, at the lowest test Mach number the stability data for the basic configuration at a 45° roll angle are presented to illustrate the effect of the asymmetry due to the auxiliary rockets for this configuration.

For subsonic, transonic, and supersonic Mach numbers up to about $M = 2.50$, the basic configuration has a higher static directional stability than longitudinal stability. At higher Mach numbers the basic configuration is more statically stable in the longitudinal plane. The data near zero angle of attack for the 45° roll angle indicate a small increase in stability over that of the basic configuration.

Comparisons of the Estimated and Measured
Aerodynamic Characteristics

It is of interest to determine the accuracy which may be obtained by using preliminary design methods for estimating the aerodynamic characteristics of the configuration. Estimates were therefore made of the aerodynamic characteristics of the fin-body combination (basic configuration with auxiliary rockets removed). It was previously pointed out that an analytic determination of the aerodynamic effects of the unusual nose on the configuration tested would be difficult if not impossible to obtain; therefore, a more conventional, blunted cone-cylinder body shape which approximates the actual shape was assumed. The assumed shape was a 15° half-angle blunted cone (radius of 0.35 inch) which terminated in the 3.1-inch diameter of the second-stage cylinder. (See sketches in fig. 9(a).)

The method of reference 2 was employed for the determination of $C_{N\alpha}$ and $\left(\frac{x_{cp}}{d}\right)_\alpha$ for the fin-body combination. Theoretical data were obtained from references 2 and 3 for the fin contribution and from references 2 and 4 for the body contribution.

The axial force $C_{A,0}$ was determined by summing the $C_{A,0}$ of the components. For the body contribution the pressure drag of the blunted conical nose and the separation band (fig. 2(a)) and the skin-friction drag were included. The pressure drag of the nose was obtained from experimental data of reference 5 and theoretical data of reference 6. The pressure drag of the separation band was obtained from experimental data in reference 7. The skin-friction drag was computed by the method of reference 8. For the fin contribution the pressure drag of the modified double-wedge profile and skin-friction drag were considered. Pressure drag for the profile was neglected at subsonic speeds, estimated from data in reference 9 at transonic speeds, and computed from linear theory at supersonic speeds. The skin friction was again computed by the method of reference 8.

Comparisons of the estimated aerodynamic characteristics with wind-tunnel measurements of the characteristics are presented in figures 9(a) to 9(c). Wind-tunnel data are presented for the fin-body combination for the entire Mach number range and for the body-alone configuration at supersonic speeds only. The fin effects at supersonic speeds were deduced from these data and are also presented. Estimates of the aerodynamic characteristics for the fin, body, and fin-body combination are presented for the Mach number range of interest. The fin contribution includes interference effects for $C_{N\alpha}$ and $\left(\frac{x_{cp}}{d}\right)_\alpha$ but does not include interference effects for $C_{A,0}$.

The comparison of the estimated $C_{N\alpha}$ with wind-tunnel measurements is shown in figure 9(a). The estimated results for all Mach numbers agree with the

measured results within the ± 10 percent accuracy range associated with the method of reference 2. The estimates at subsonic and transonic speeds are in general about 10 percent higher than the measured data. At supersonic Mach numbers the estimates are in very good agreement with the measured data. The comparison for the center of pressure $\left(\frac{x_{cp}}{d}\right)_a$

is shown in figure 9(b). The accuracy range quoted in reference 2 for the $\left(\frac{x_{cp}}{d}\right)_a$ estimates, in terms of body

diameters of the present configuration, is ± 0.31 . The results indicate an estimated $\left(\frac{x_{cp}}{d}\right)_a$ of as much as 0.8 diameter aft of the measured data at subsonic

Mach numbers. This difference between estimated and measured data decreases with Mach number and becomes constant at about 0.3 diameter for transonic and supersonic Mach numbers. The results of the comparison for the stability data

$(C_{N_a} \text{ and } \left(\frac{x_{cp}}{d}\right)_a)$ indicate that, except for $\left(\frac{x_{cp}}{d}\right)_a$ at subsonic speeds, the

estimates agree with measured data within the specified accuracy limits. The assumption of a simplified body shape therefore resulted in a reasonable prediction of the static stability of the fin-body configuration.

The results for the axial force $C_{A,0}$ are presented in figure 9(c). There is good agreement between the estimated and measured data for the fin-body combination at subsonic and transonic speeds and very poor agreement at supersonic speeds. The fin data at supersonic speeds indicate estimates which are somewhat low particularly at the higher Mach numbers. This result is to be expected since fin-interference effects were not included in the estimates and there was some bluntness at the fin leading edge which was not accounted for in the axial-force estimations. The estimated data for the body alone at supersonic speeds are considerably lower than the measured data. The differences in these data are as much as 35 percent ($M = 2.30$). The results of the comparison therefore indicate that the assumption of the simplified body is inadequate for predicting the axial force of the fin-body configuration.

CONCLUSIONS

An investigation has been conducted in various wind-tunnel facilities at the Langley Research Center to determine the aerodynamic characteristics of a 0.10-scale model of a two-stage rocket vehicle. The aerodynamic characteristics of the model were obtained for subsonic, transonic, and supersonic Mach numbers. The effects of two auxiliary rockets attached to the sides of the first stage were determined at subsonic, transonic, and supersonic speeds. The effects of four control rocket fairings at the nose were determined for supersonic speeds. The body-alone configuration was also tested at supersonic Mach numbers so that the fin and body contributions could be determined. In addition to providing

aerodynamic data for trajectory simulations and the determination of aerodynamic loads, this investigation indicated the following conclusions:

1. The presence of the auxiliary rockets on the sides of the model caused small (less than 10 percent) changes in the static longitudinal stability level near zero angle of attack at all Mach numbers. At subsonic speeds and high angles of attack the rockets caused significant increases in the stability level. The effects of the auxiliary rockets on the directional stability level near zero angle of sideslip were negligible.
2. The aerodynamic asymmetry in the roll plane resulting from the auxiliary rockets causes the aerodynamic characteristics to vary with roll angle. For example, near zero angle of attack and sideslip the longitudinal stability (corresponds to 0° roll angle) is up to 10 percent lower than the directional stability (corresponds to 90° roll angle) at Mach numbers up to about 2.5 and the longitudinal stability is as much as 20 percent higher than the directional stability at higher Mach numbers. At subsonic speeds a 45° roll results in a small increase in stability near zero angle of attack. At high angles of attack the 45° roll angle results in a significant decrease in stability level.
3. The presence of the auxiliary rockets caused an increase in axial force of between 12 and 16 percent except in the drag rise region where the increase was about 6 percent.
4. The presence of the control rocket fairings resulted in a decrease in static longitudinal and directional stabilities of up to 15 percent at supersonic speeds.
5. The fairings caused an increase in axial force of up to 13 percent at the supersonic test Mach numbers.
6. The results of a comparison of estimated and measured fin and body aerodynamic characteristics indicated that reasonable estimates could be made of the effect of the fins on the static stability and axial-force characteristics. By assuming a simplified shape for the body, reasonable estimates were made for the body contribution to the static stability; however, this assumption leads to estimates of the axial force which were considerably lower than the measured values.

Langley Research Center,
National Aeronautics and Space Administration,
Langley Station, Hampton, Va., July 20, 1964.

REFERENCES

1. Young, A. Thomas, and Harris, Jack E.: An Analog Study of a Rotating-Solid-Rocket Control System and Its Application to Attitude Control of a Space-Vehicle Upper Stage. NASA TN D-2366, 1964.
2. Pitts, William C., Nielsen, Jack N., and Kaattari, George E.: Lift and Center of Pressure of Wing-Body-Tail Combinations at Subsonic, Transonic, and Supersonic Speeds. NACA Rep. 1307, 1957.
3. DeYoung, John, and Harper, Charles W.: Theoretical Symmetric Span Loading at Subsonic Speeds for Wings Having Arbitrary Plan Form. NACA Rep. 921, 1948.
4. Syvertson, Clarence A., and Dennis, David H.: A Second-Order Shock-Expansion Method Applicable to Bodies of Revolution Near Zero Lift. NACA Rep. 1328, 1957. (Supersedes NACA TN 3527.)
5. Geudtner, W. J., Jr.: Sharp and Blunted Cone Force Coefficients and Centers of Pressure From Wind Tunnel Tests at Mach Numbers From 0.50 to 4.06. Rep. No. ZA-7-017, Convair/Astronautics, June 16, 1955.
6. Staff of the Computing Section, Center of Analysis (Under Direction of Zdeněk Kopal): Tables of Supersonic Flow Around Yawing Cones. Tech. Rep. No. 3 (N0rd Contract No. 9169), M.I.T., 1947.
7. Hoerner, Sighard F.: Fluid-Dynamic Drag. Publ. by the author (148 Busteed Drive, Midland Park, N.J.), 1958.
8. Chin, S. S.: Missile Configuration Design. McGraw-Hill Book Co., Inc., c.1961.
9. Spreiter, John R.: On the Application of Transonic Similarity Rules to Wings of Finite Span. NACA Rep. 1153, 1953. (Supersedes NACA TN 2726.)

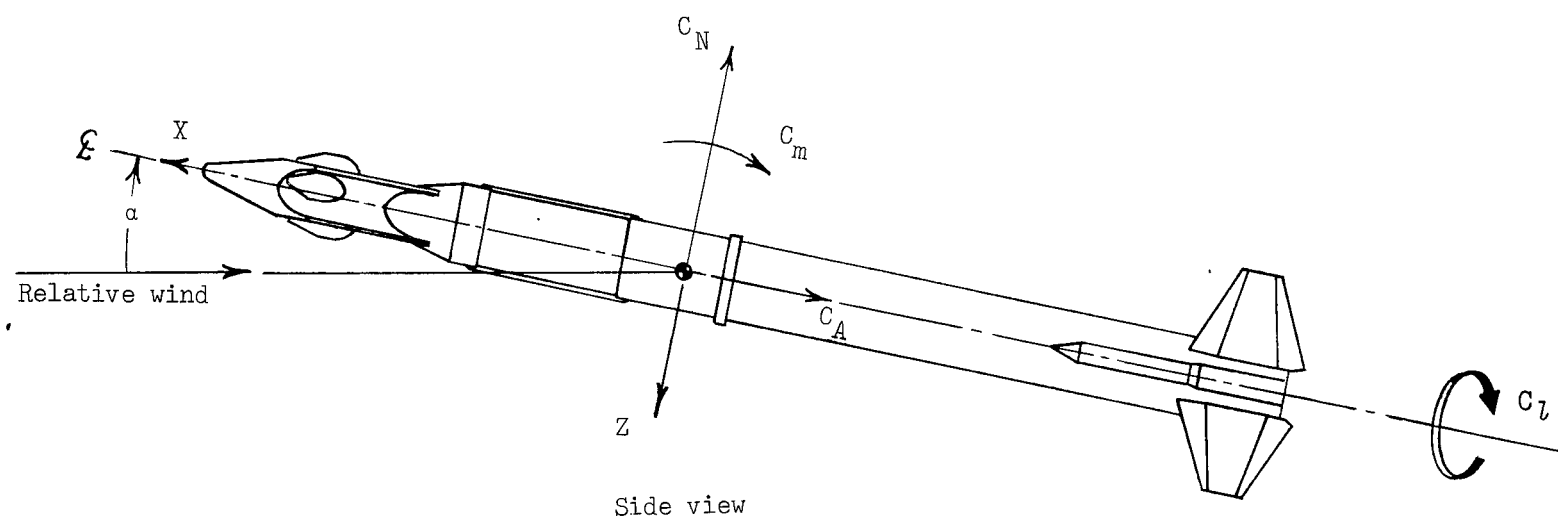
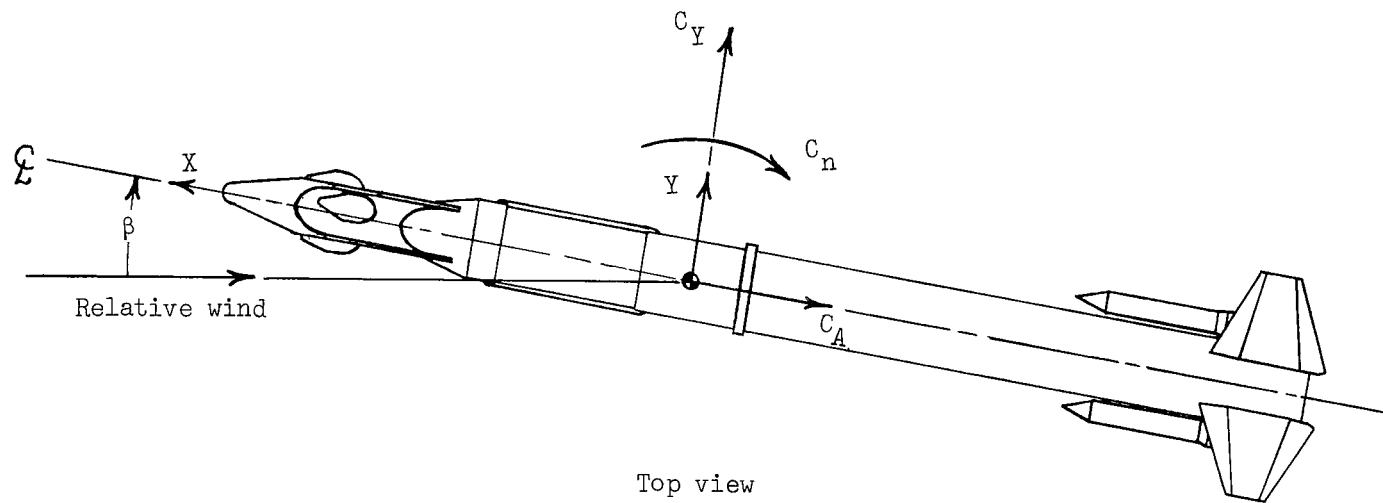
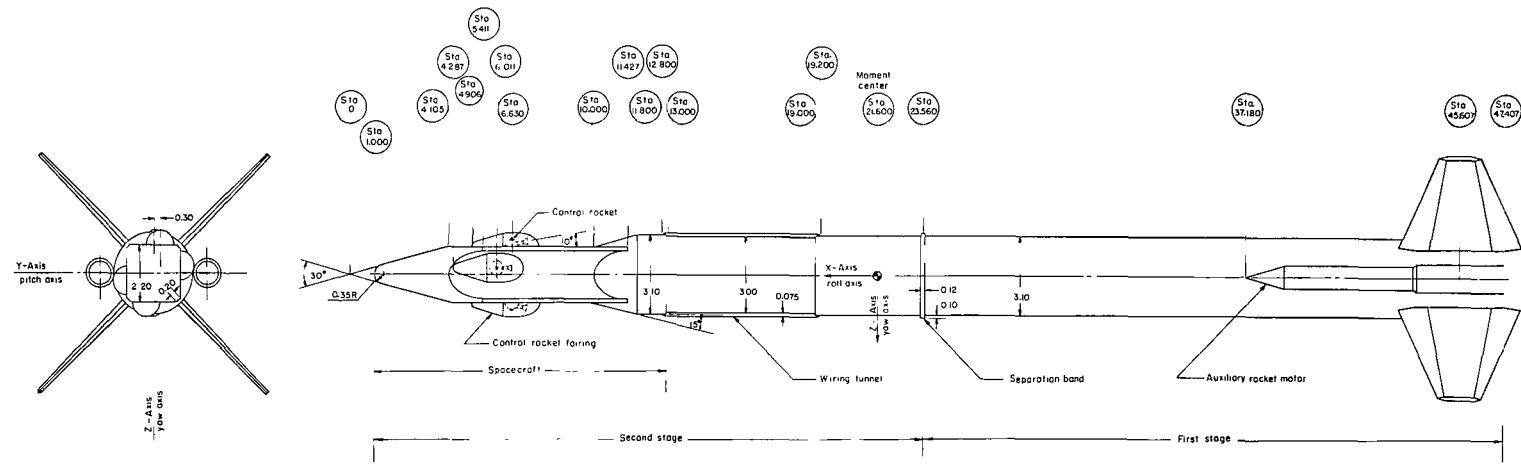
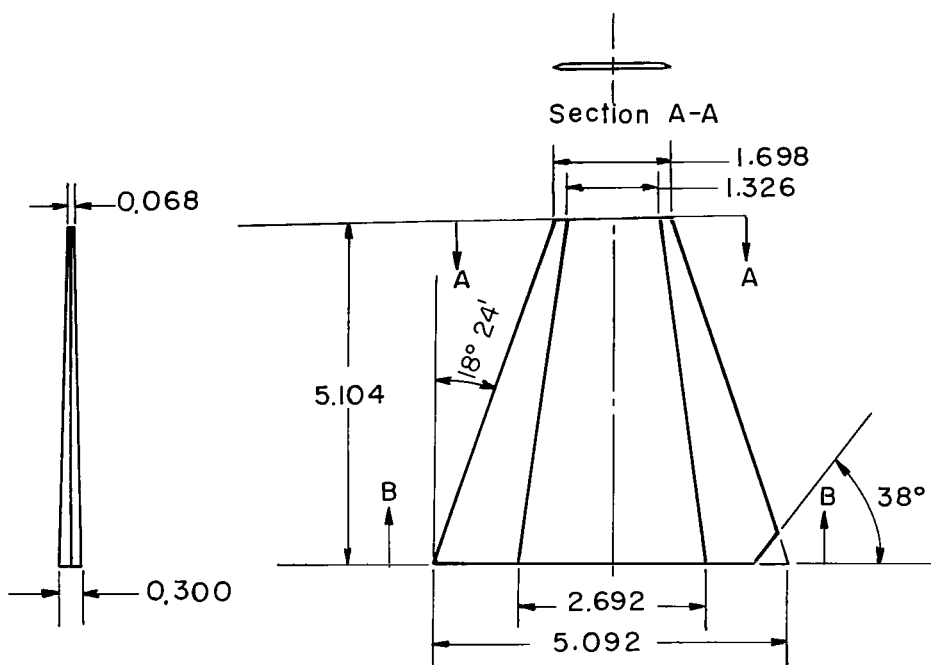


Figure 1.- Body-axis system. Arrows indicate positive directions.

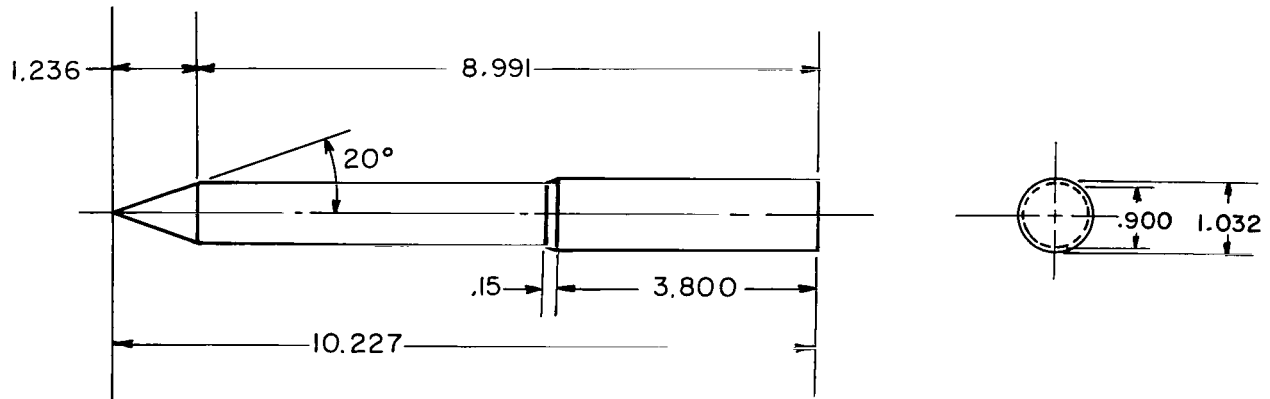


(a) Sketch of basic configuration. Circled numbers indicate station in inches.

Figure 2.- Details and dimensions of model tested. All dimensions are in inches unless otherwise noted.



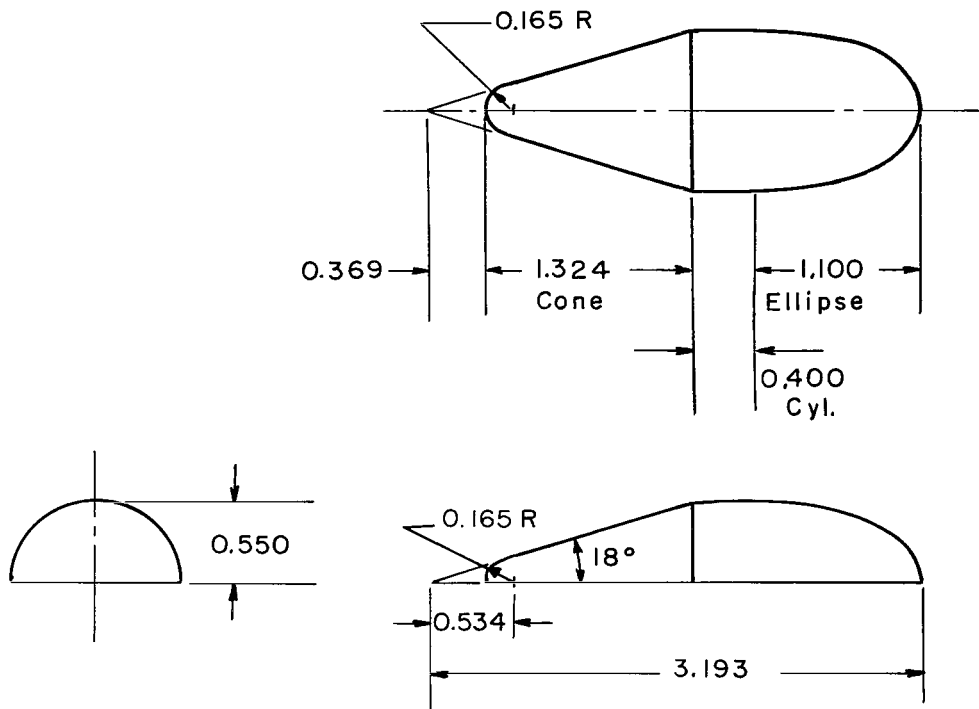
Fin panel



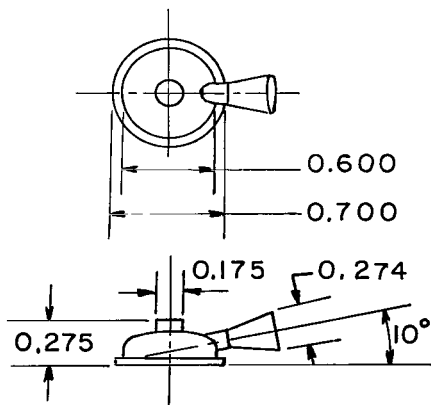
First-stage auxiliary rocket motor

(b) Sketch of fin panel and first-stage auxiliary rocket motor.

Figure 2.- Continued.



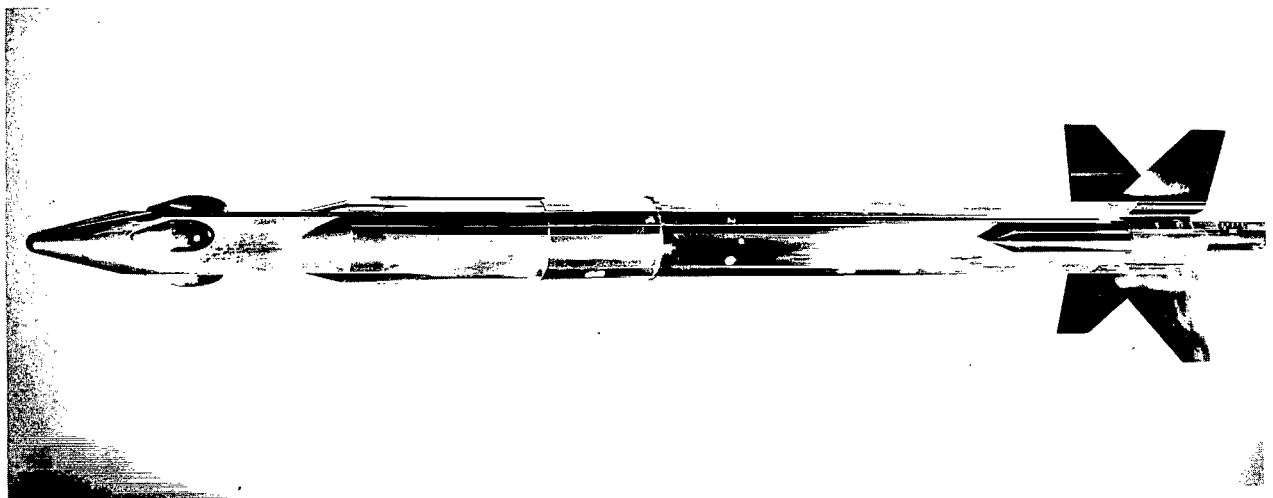
Control-rocket fairing



Control-rocket headcap

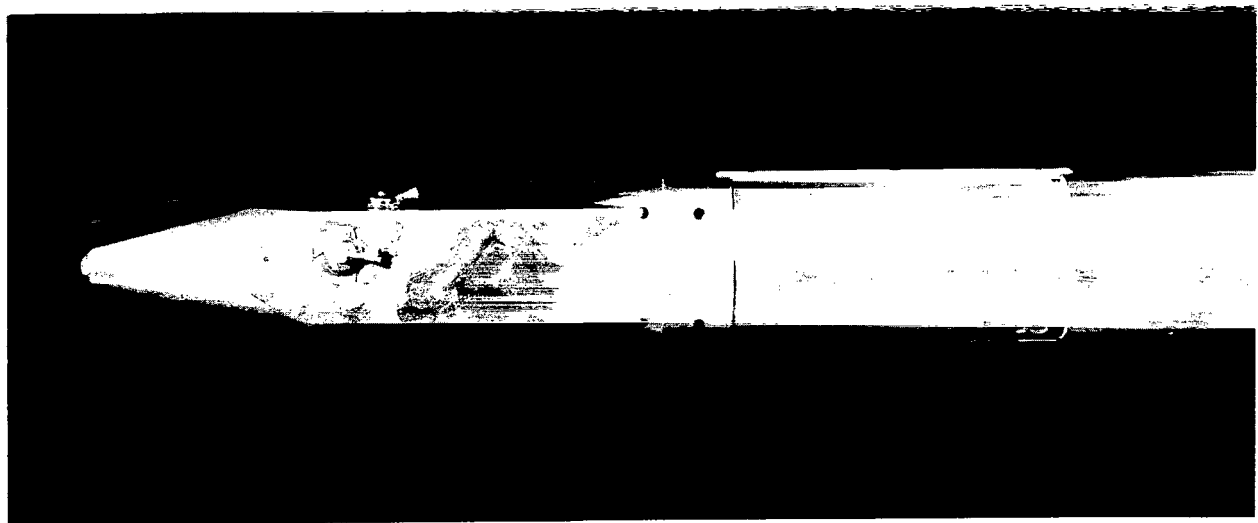
(c) Sketch of control-rocket fairing and control-rocket headcap.

Figure 2.- Concluded.



(a) Basic configuration.

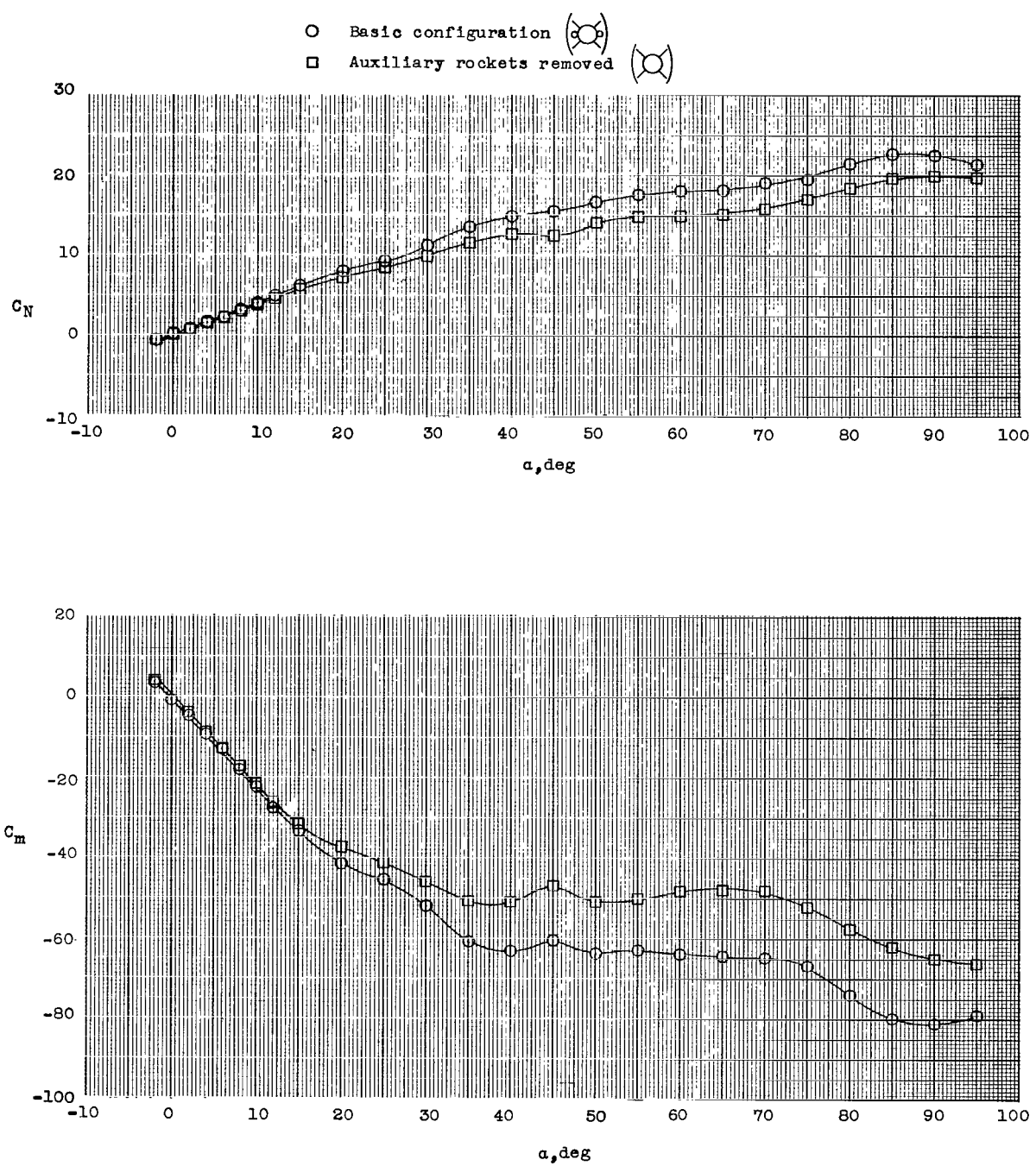
L-62-6675



(b) Closeup of nose section with control-rocket fairings removed.

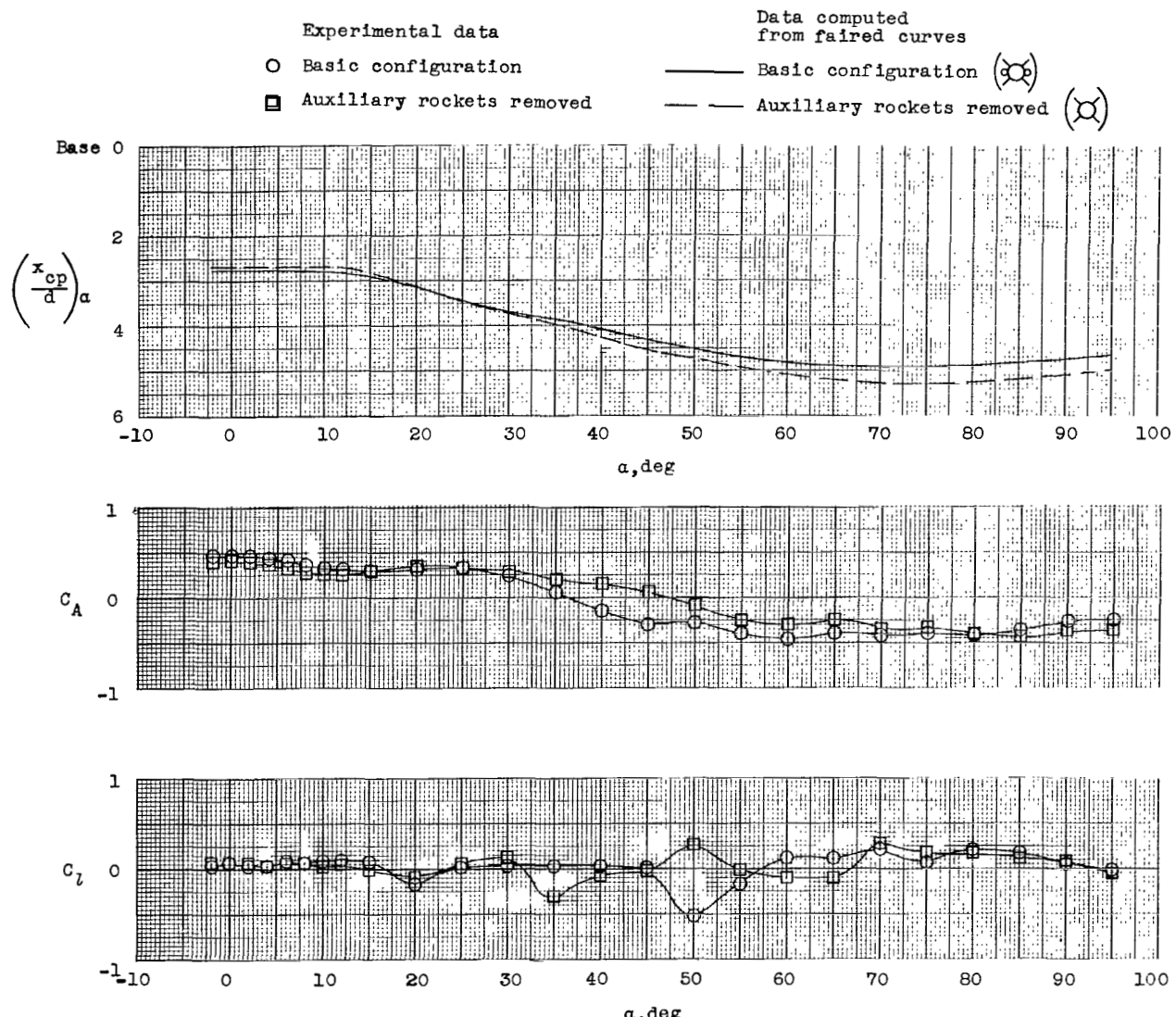
L-62-7993

Figure 3.- Photographs of model tested.



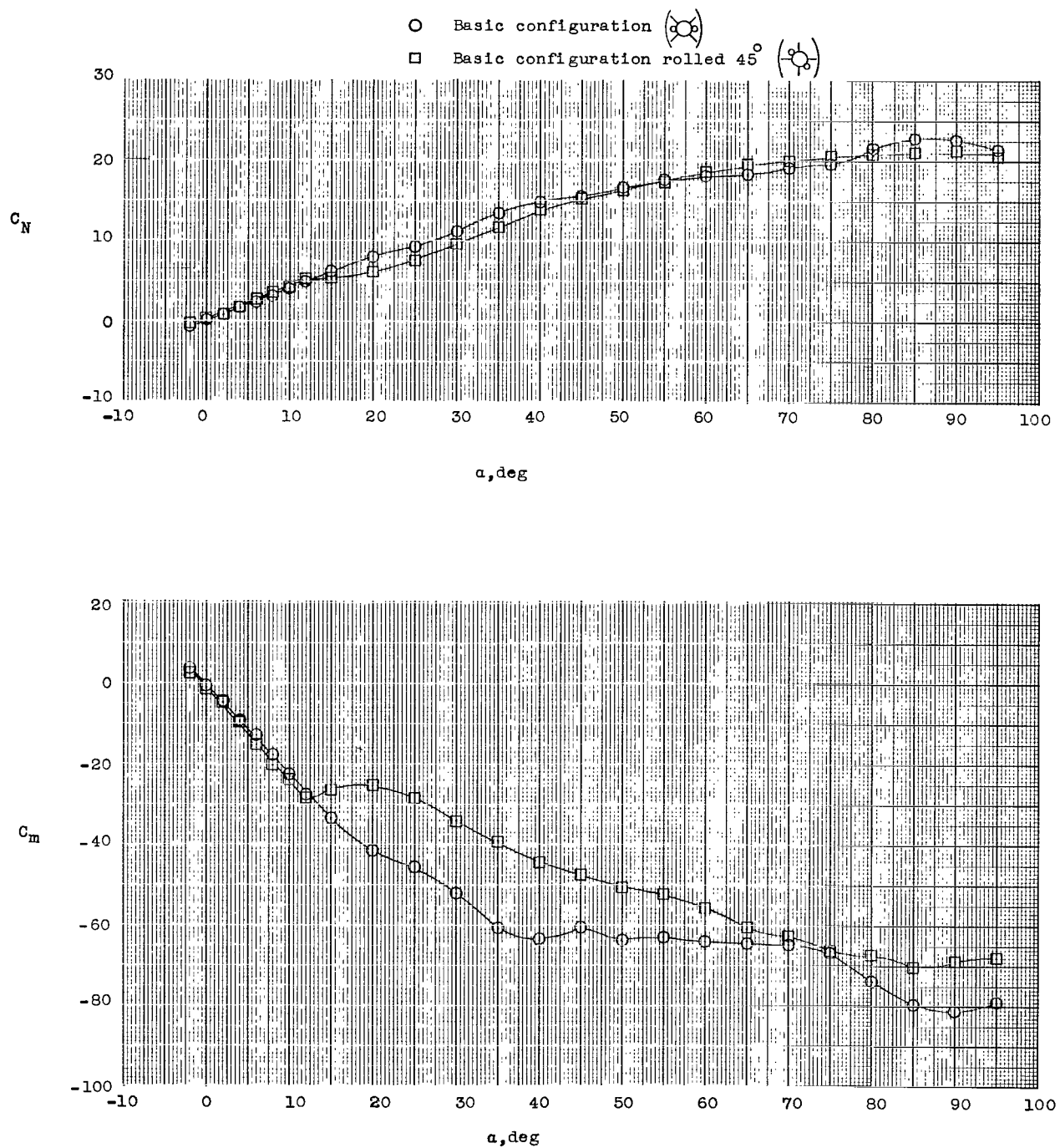
(a) Effect of auxiliary rockets on C_N and C_m .

Figure 4.- Subsonic aerodynamic characteristics of basic configuration with the effect of auxiliary rockets and roll orientation. $M = 0.22$; $\beta \approx 0^\circ$.



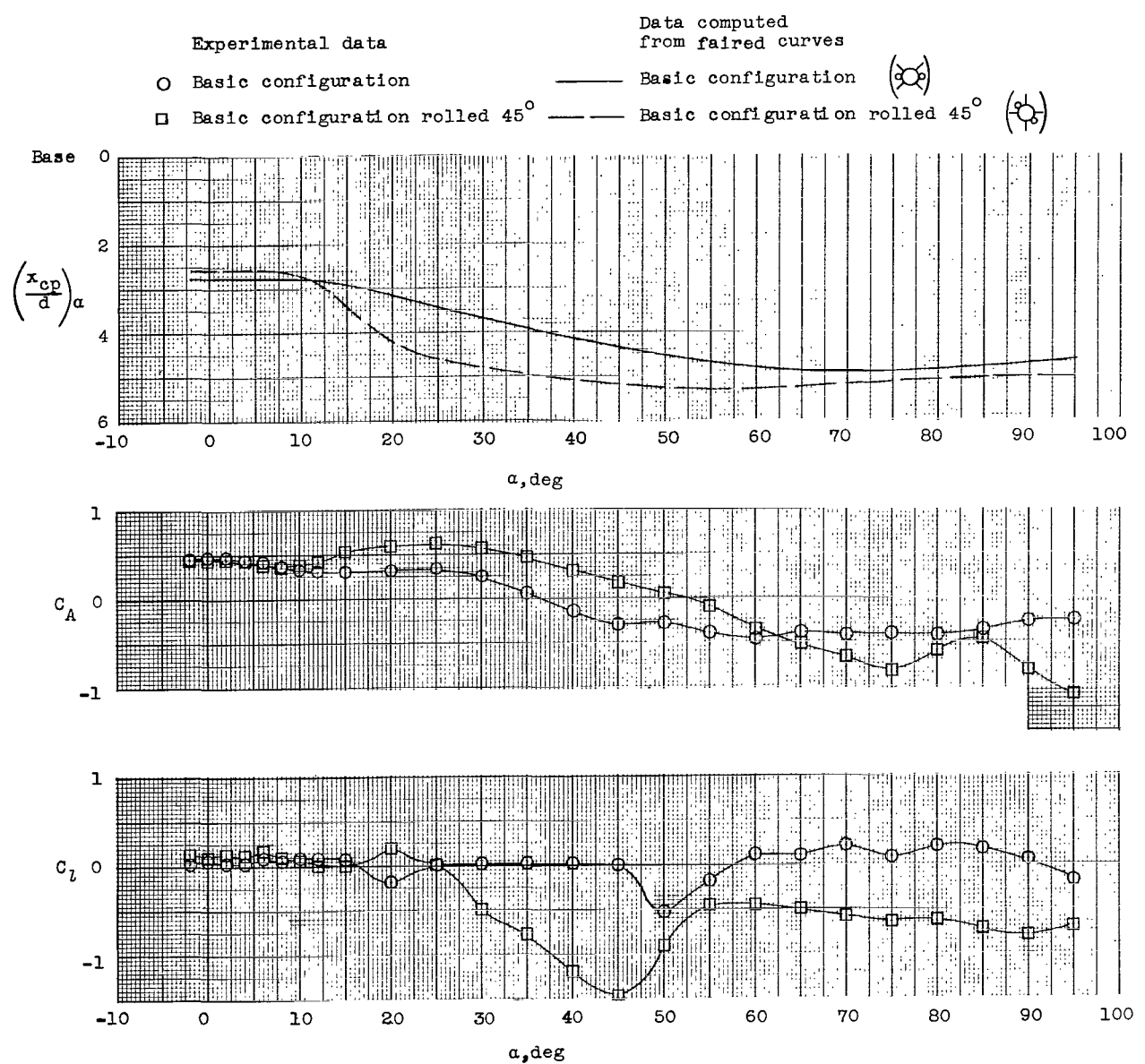
(b) Effect of auxiliary rockets on $\left(\frac{x_{cp}}{d}\right)_\alpha$, C_A , and C_l .

Figure 4.- Continued.



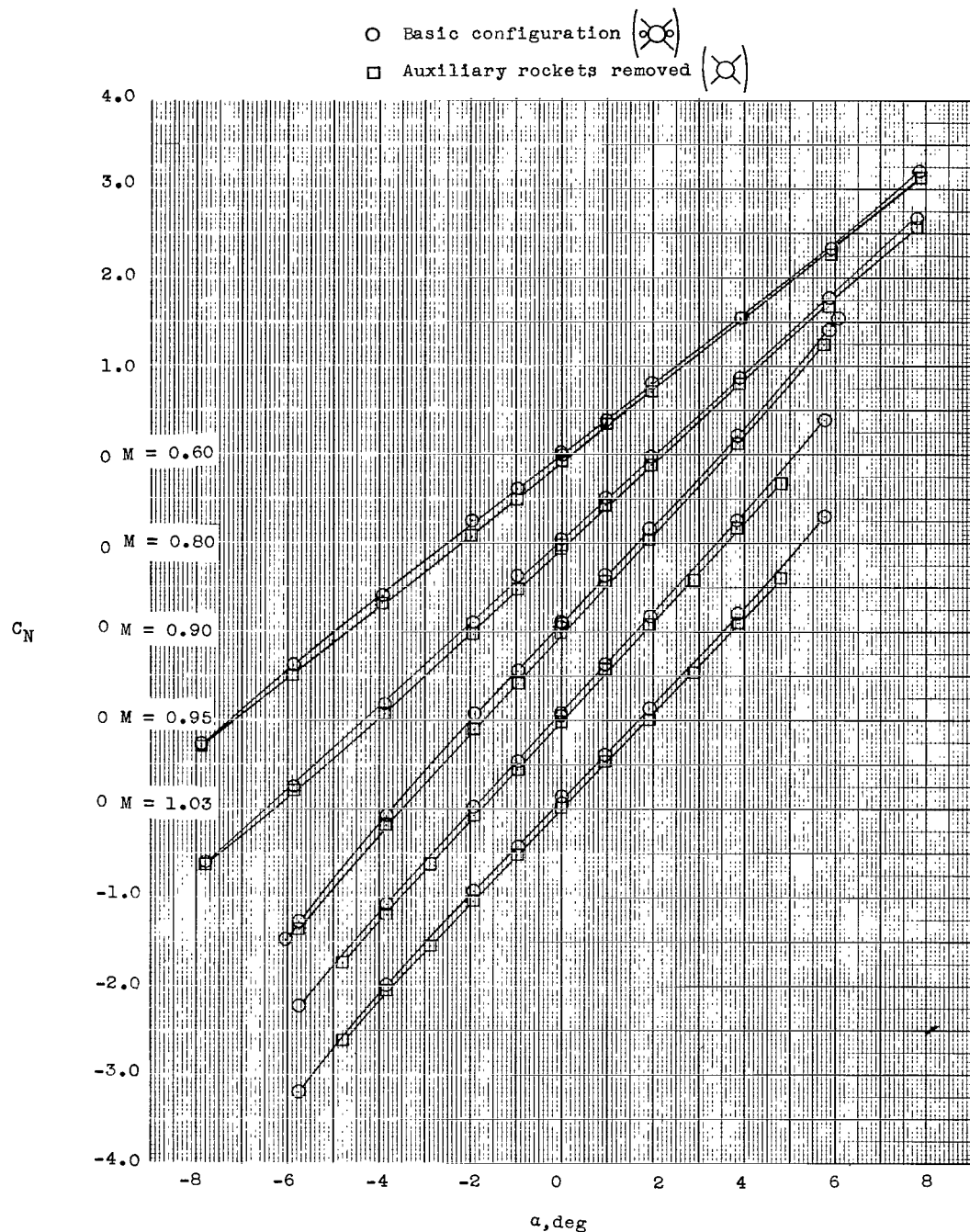
(c) Effect of roll orientation on C_N and C_m .

Figure 4.- Continued.



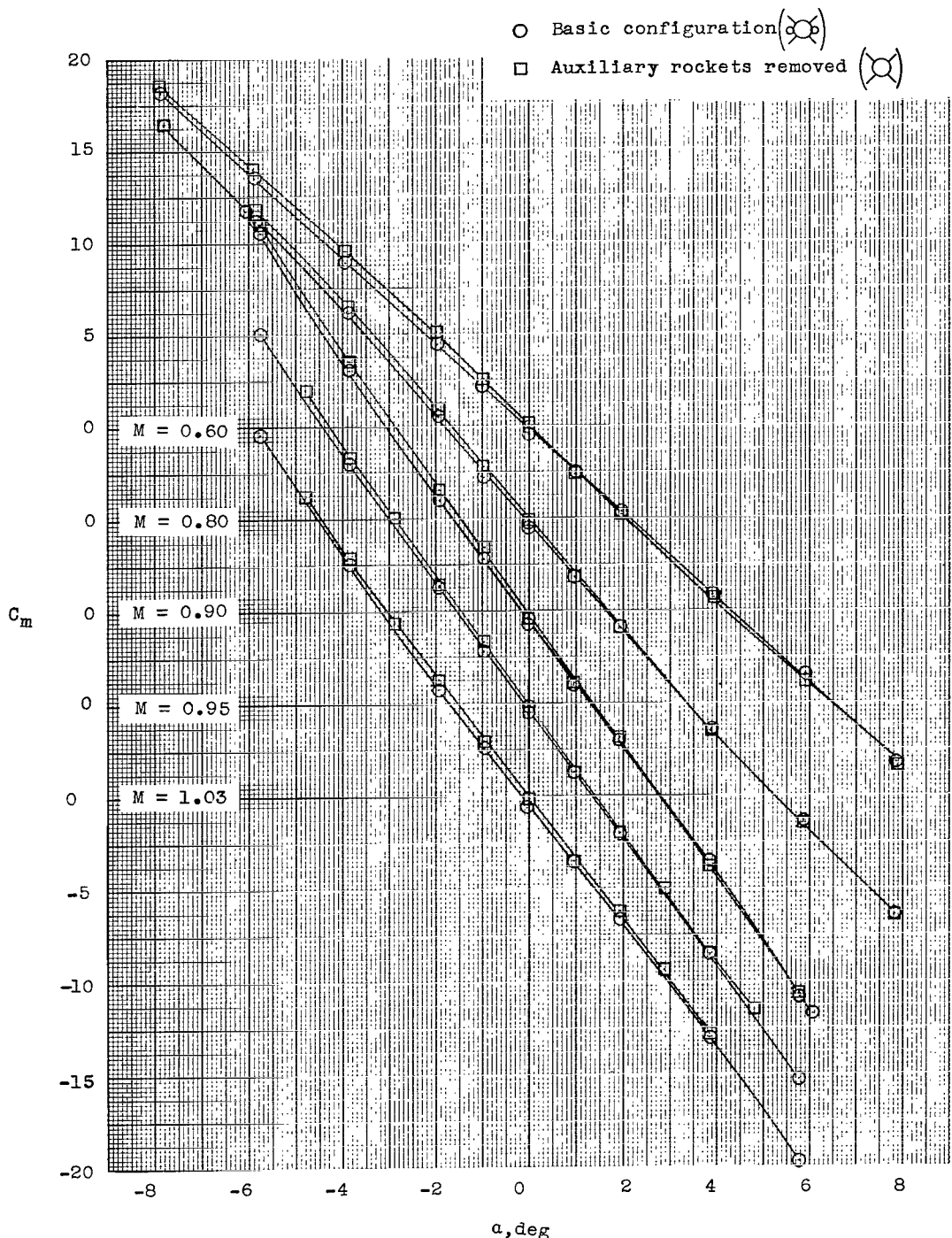
(d) Effect of roll orientation on $\left(\frac{x_{cp}}{d}\right)_\alpha$, c_A , and c_l .

Figure 4.- Concluded.



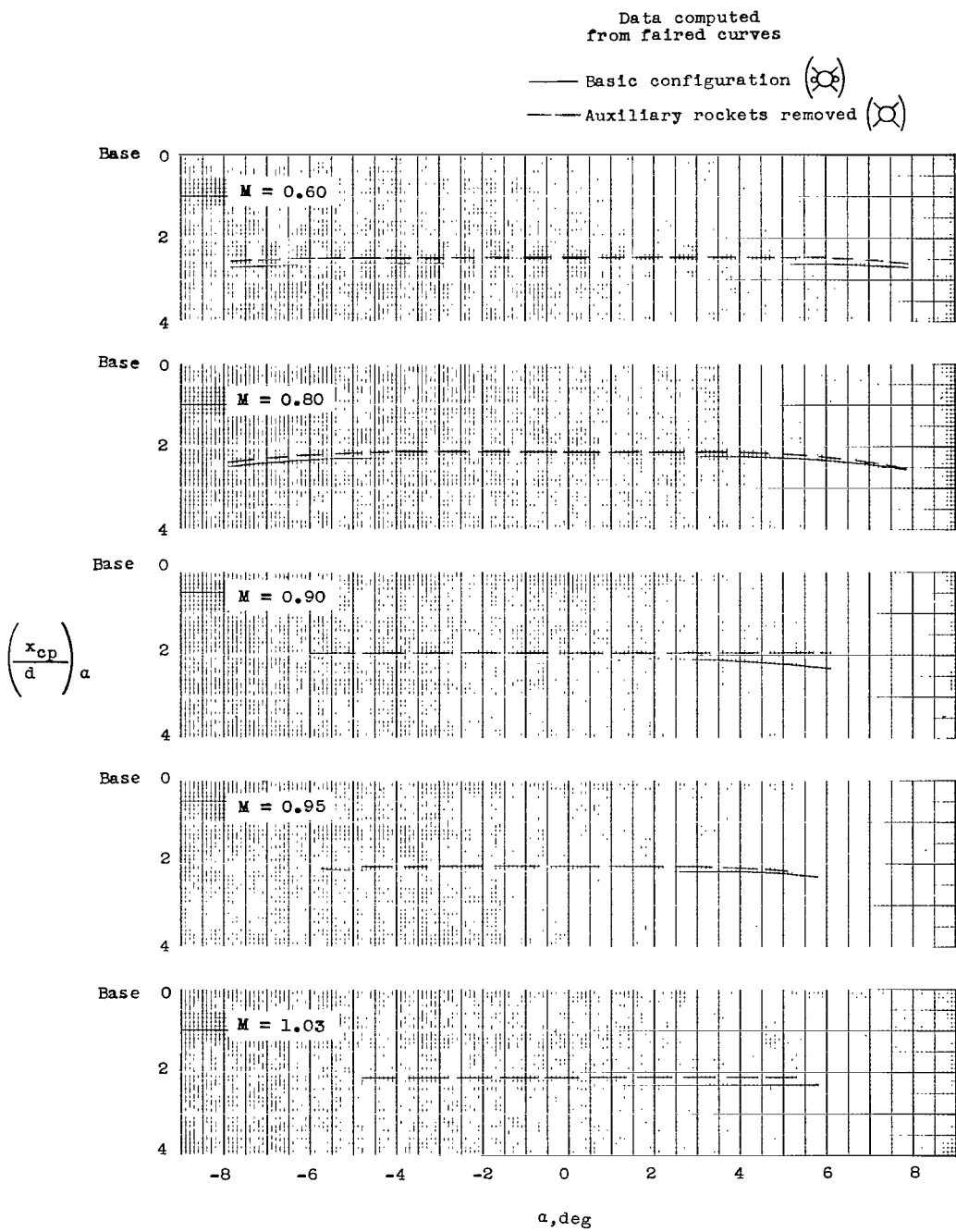
(a) C_N ; $\beta \approx 0^\circ$.

Figure 5.- Transonic aerodynamic characteristics of basic configuration and effect of auxiliary rockets.



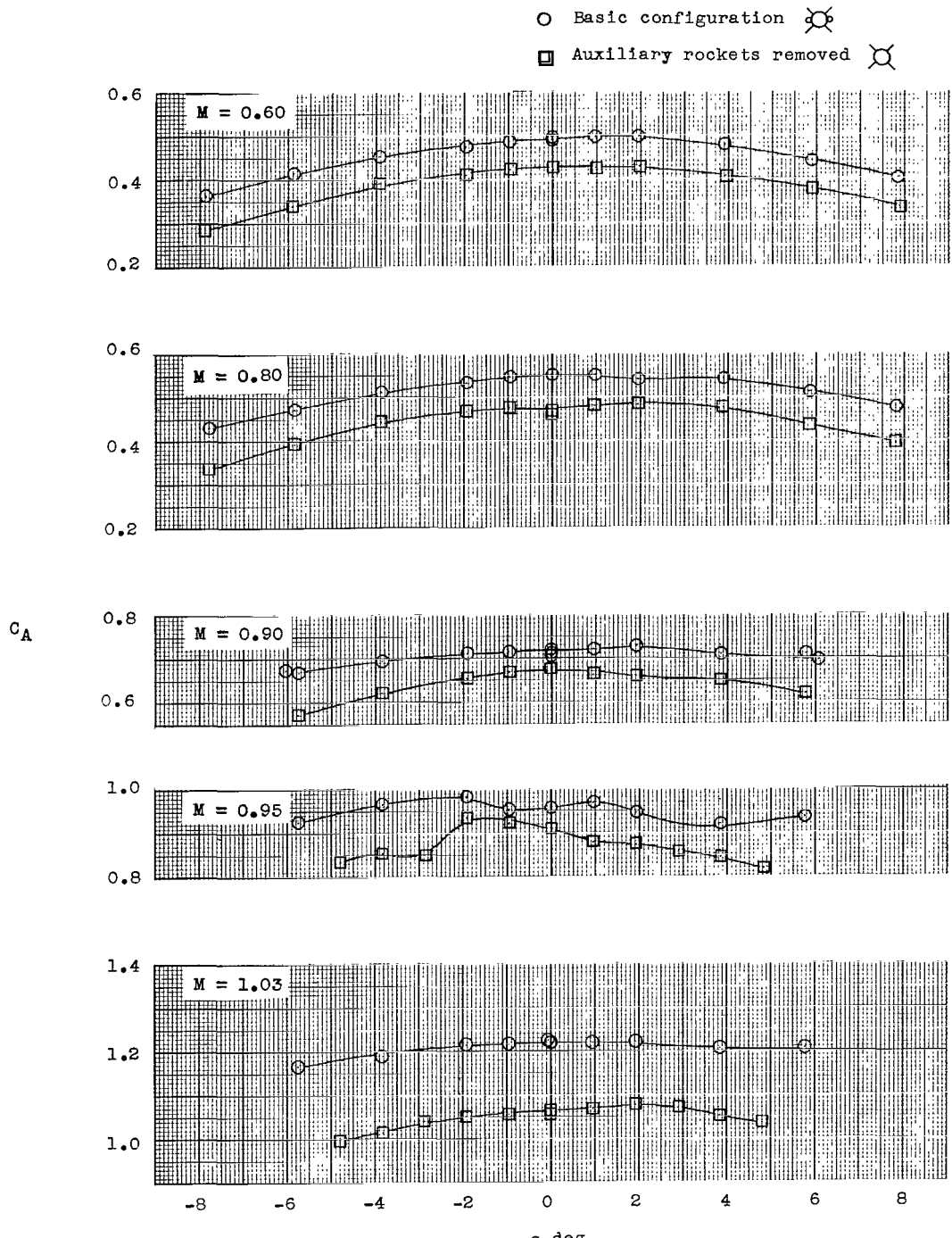
(b) C_m ; $\beta \approx 0^\circ$.

Figure 5.- Continued.



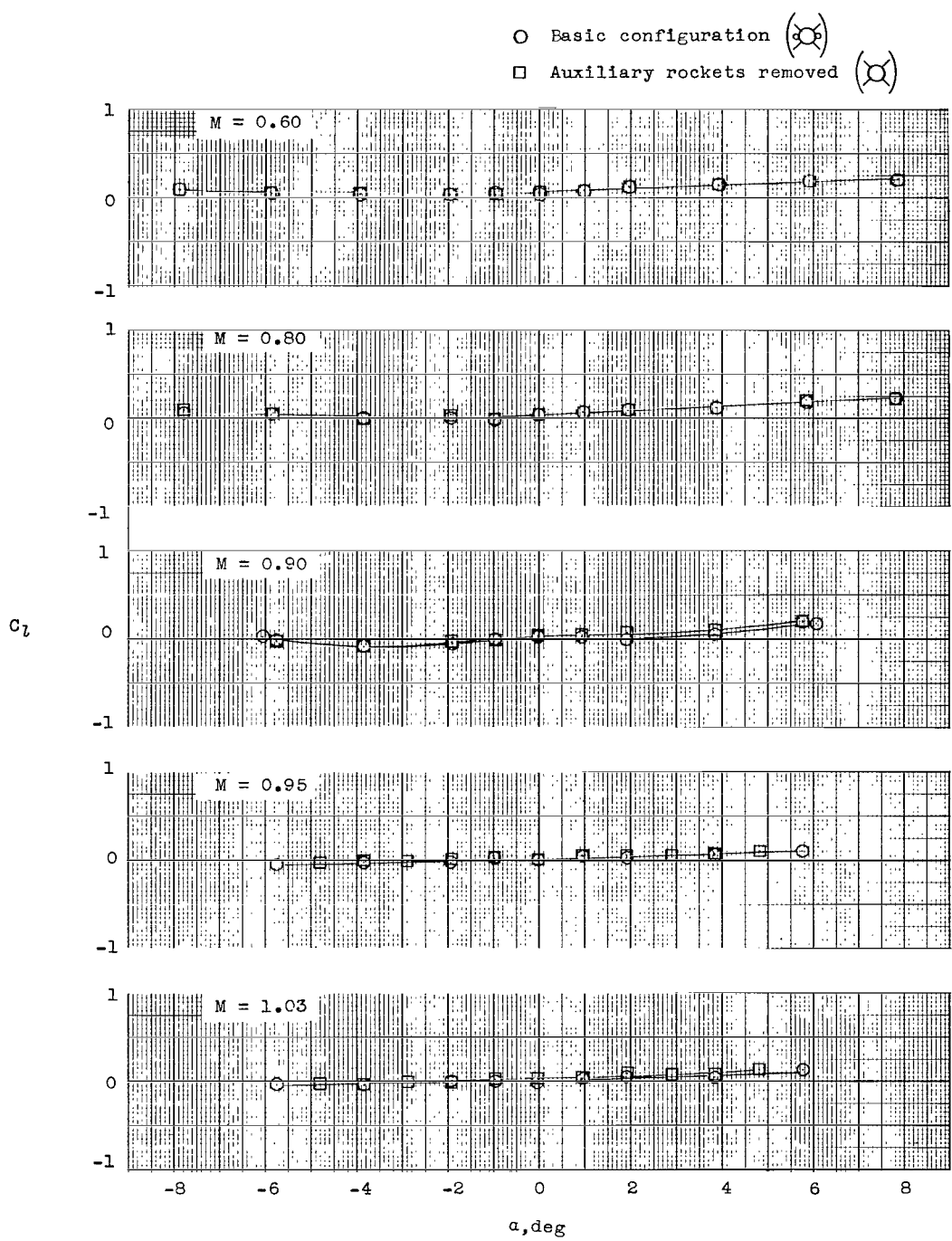
$$(c) \quad \left(\frac{x_{cp}}{d}\right)_a; \quad \beta \approx 0^\circ.$$

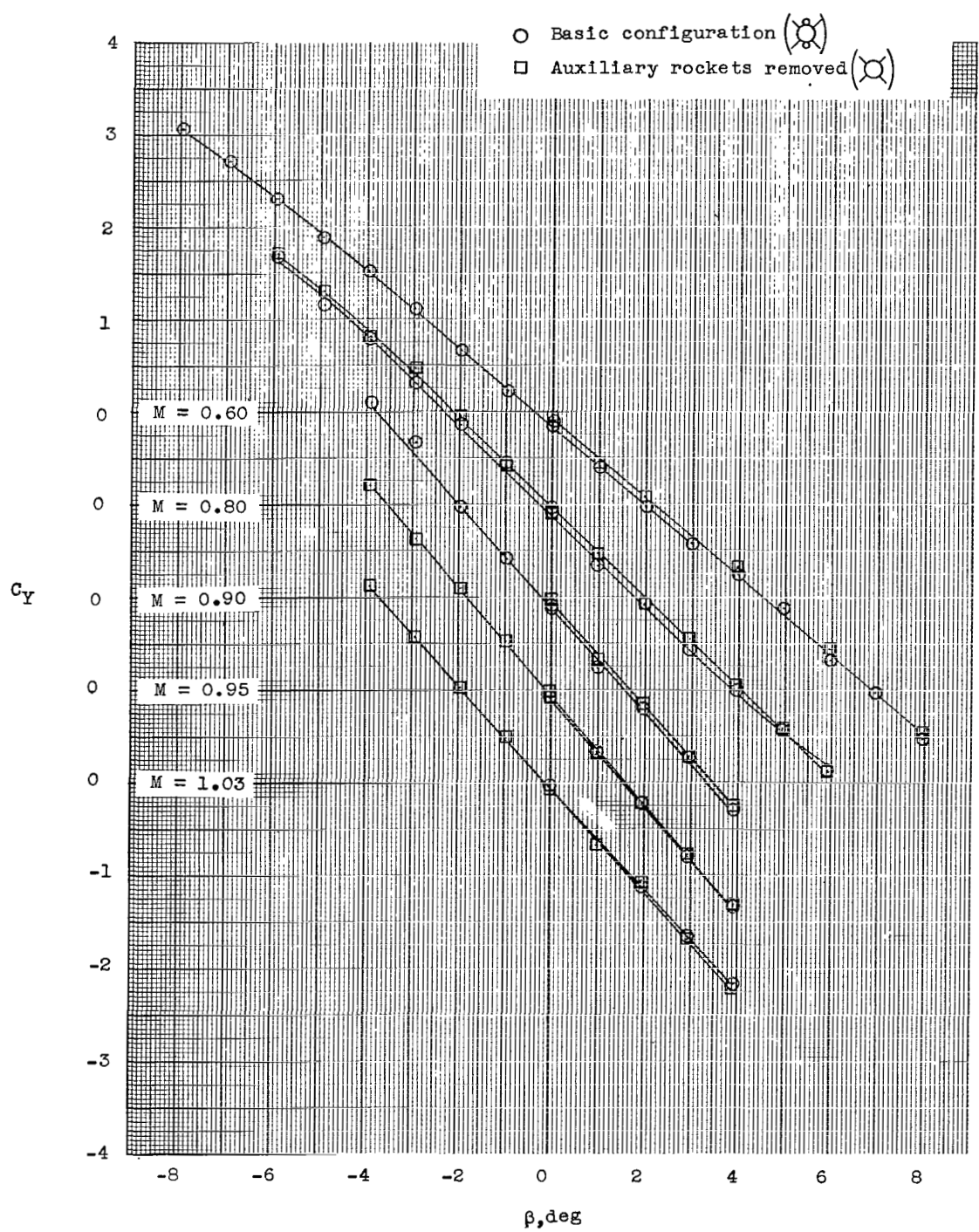
Figure 5.- Continued.



(d) C_A ; $\beta \approx 0^\circ$.

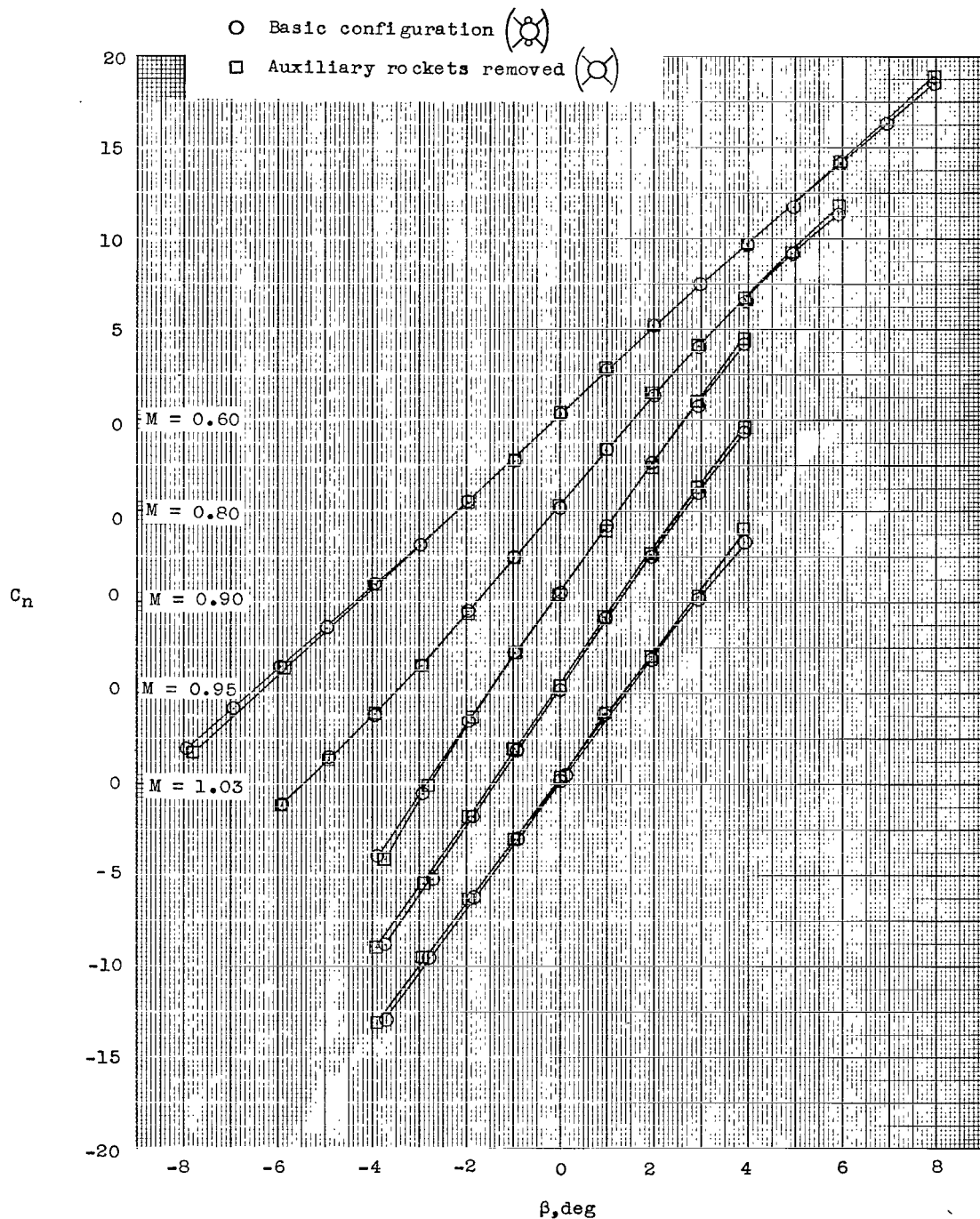
Figure 5.- Continued.





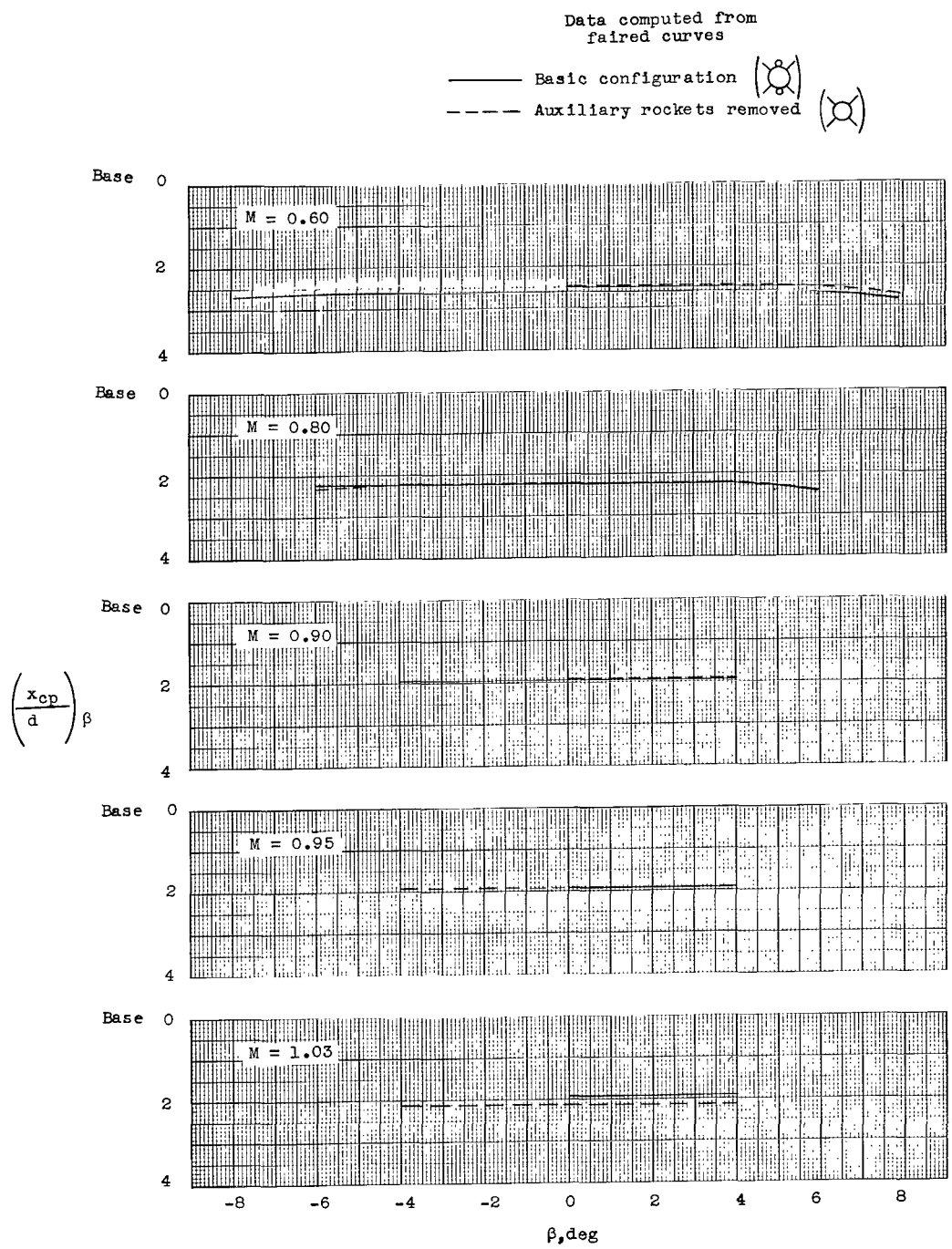
(f) C_Y ; $\alpha \approx 0^\circ$.

Figure 5.- Continued.



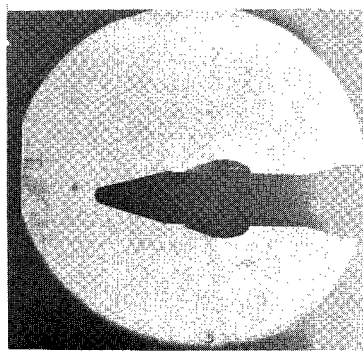
(g) C_n ; $\alpha \approx 0^\circ$.

Figure 5.- Continued.

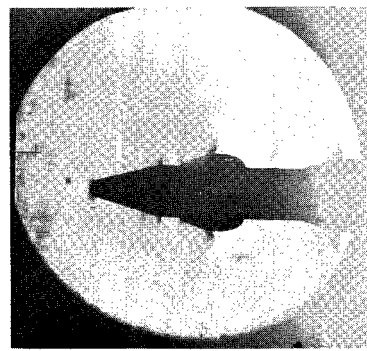


$$(h) \quad \left(\frac{x_{cp}}{d}\right)_\beta; \quad \alpha \approx 0^\circ.$$

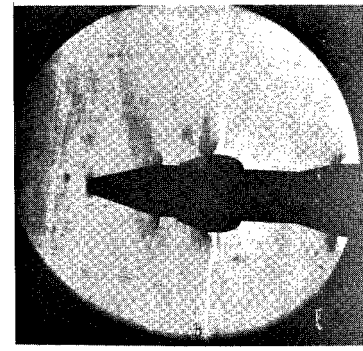
Figure 5.- Continued.



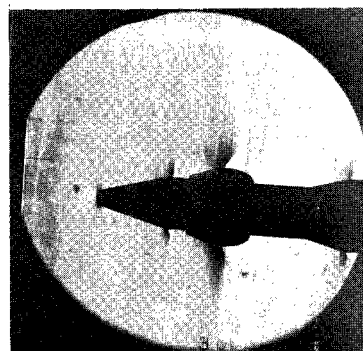
$\alpha \approx 0^\circ ; M = 0.60$



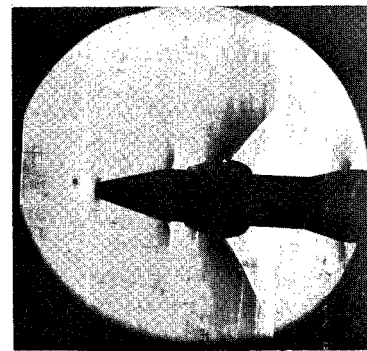
$\alpha \approx 0^\circ ; M = 0.80$



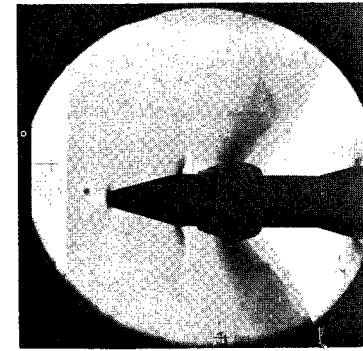
$\alpha \approx 0^\circ ; M = 0.85$



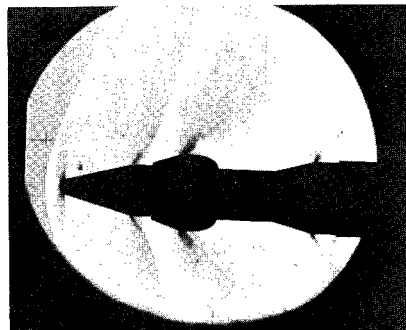
$\alpha \approx 0^\circ ; M = 0.90$



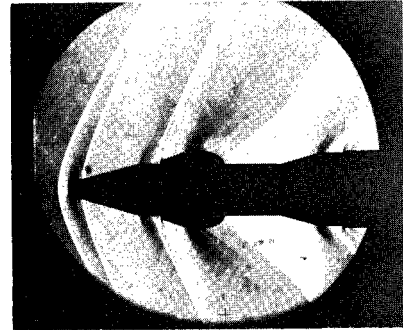
$\alpha \approx 0^\circ ; M = 0.95$



$\alpha \approx 0^\circ ; M = 1.03$



$\alpha \approx 0^\circ ; M = 1.10$

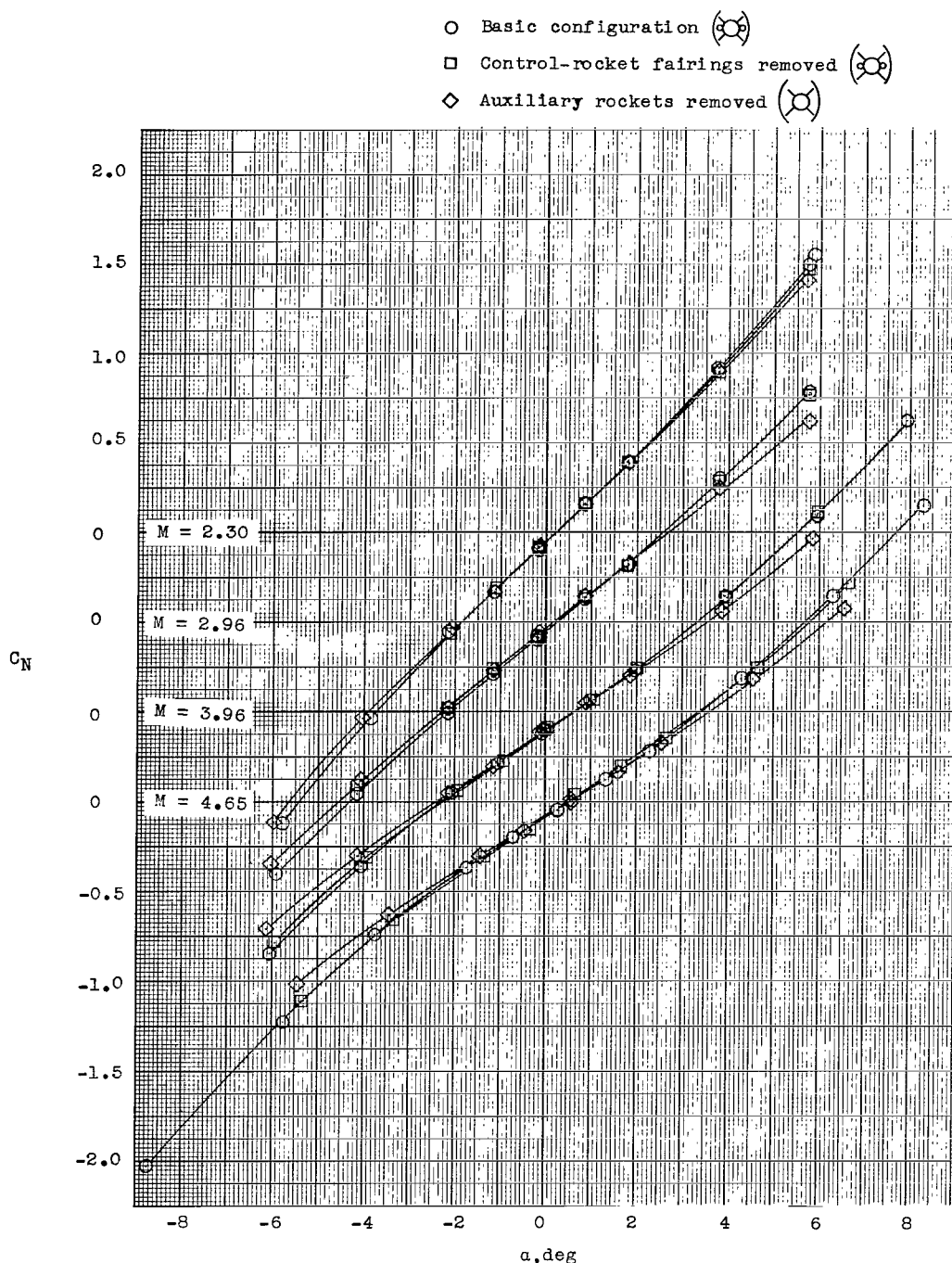


$\alpha \approx 0^\circ ; M = 1.20$

(i) Schlieren photographs of transonic flow over nose section.

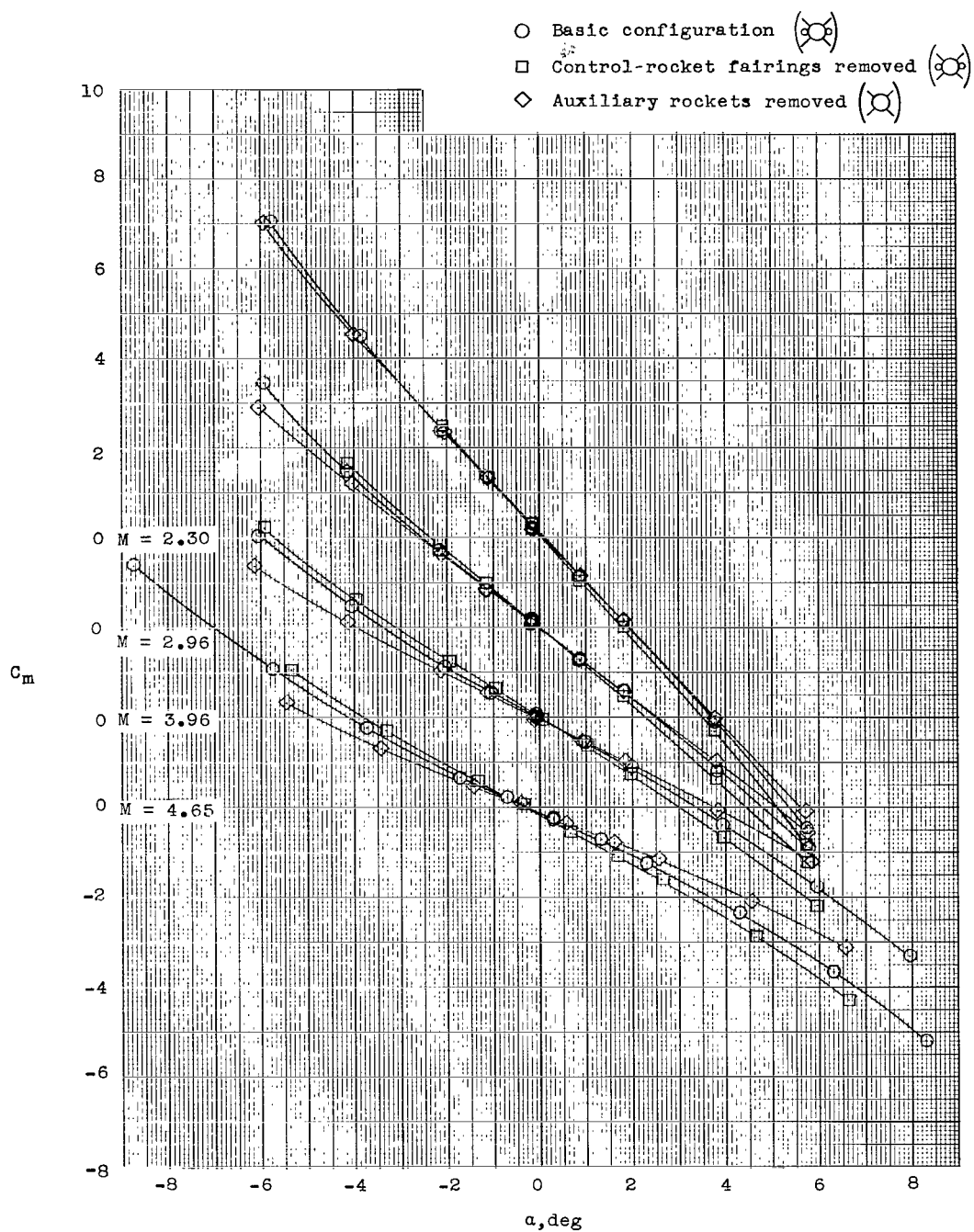
L-64-4751

Figure 5.- Concluded.



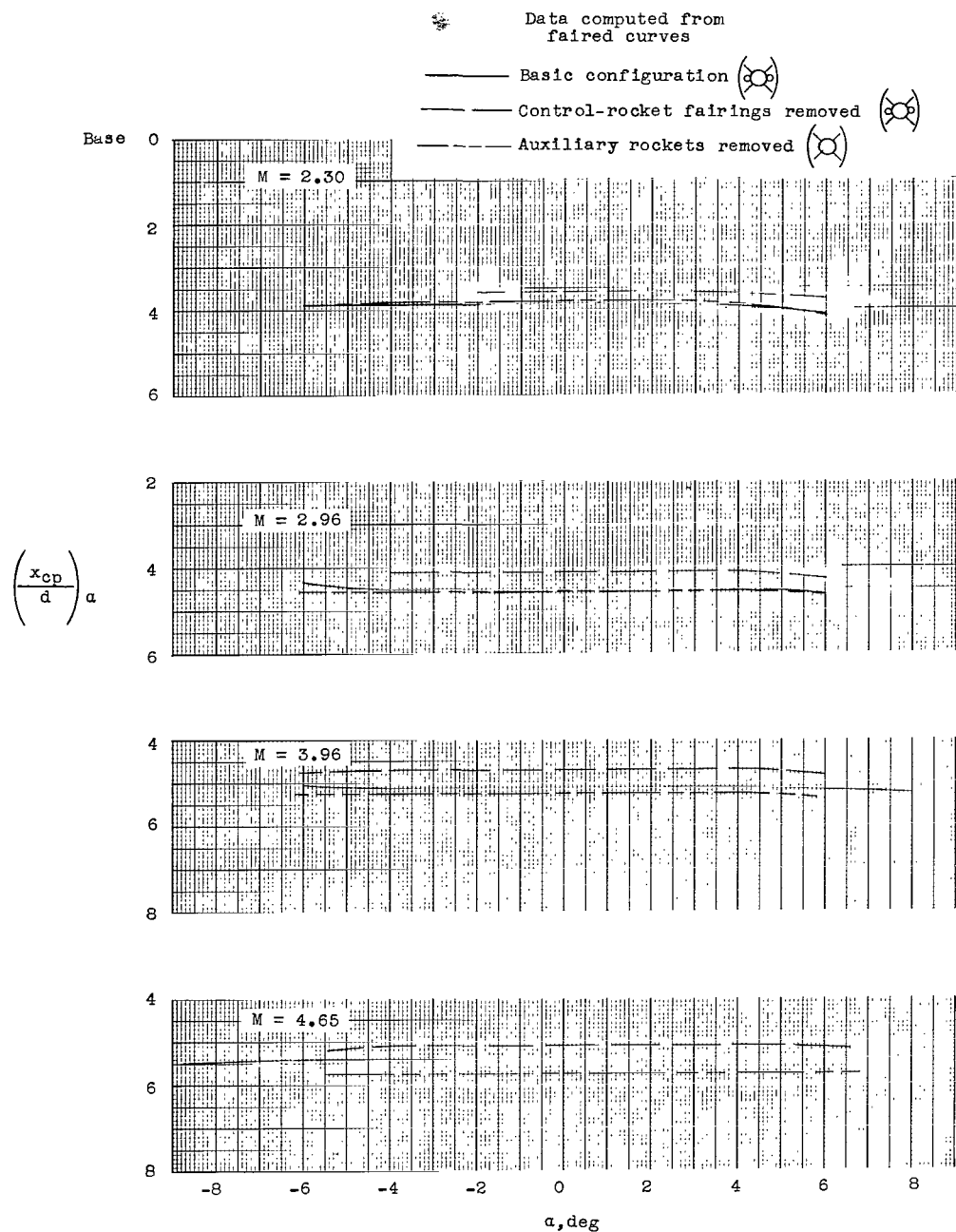
(a) C_N of basic configuration and effect on control-rocket fairings and auxiliary rockets.
 $\beta \approx 0^\circ$.

Figure 6.- Supersonic aerodynamic characteristics of basic configuration and body alone (with fairings) with the effect of control-rocket fairings and auxiliary rockets.



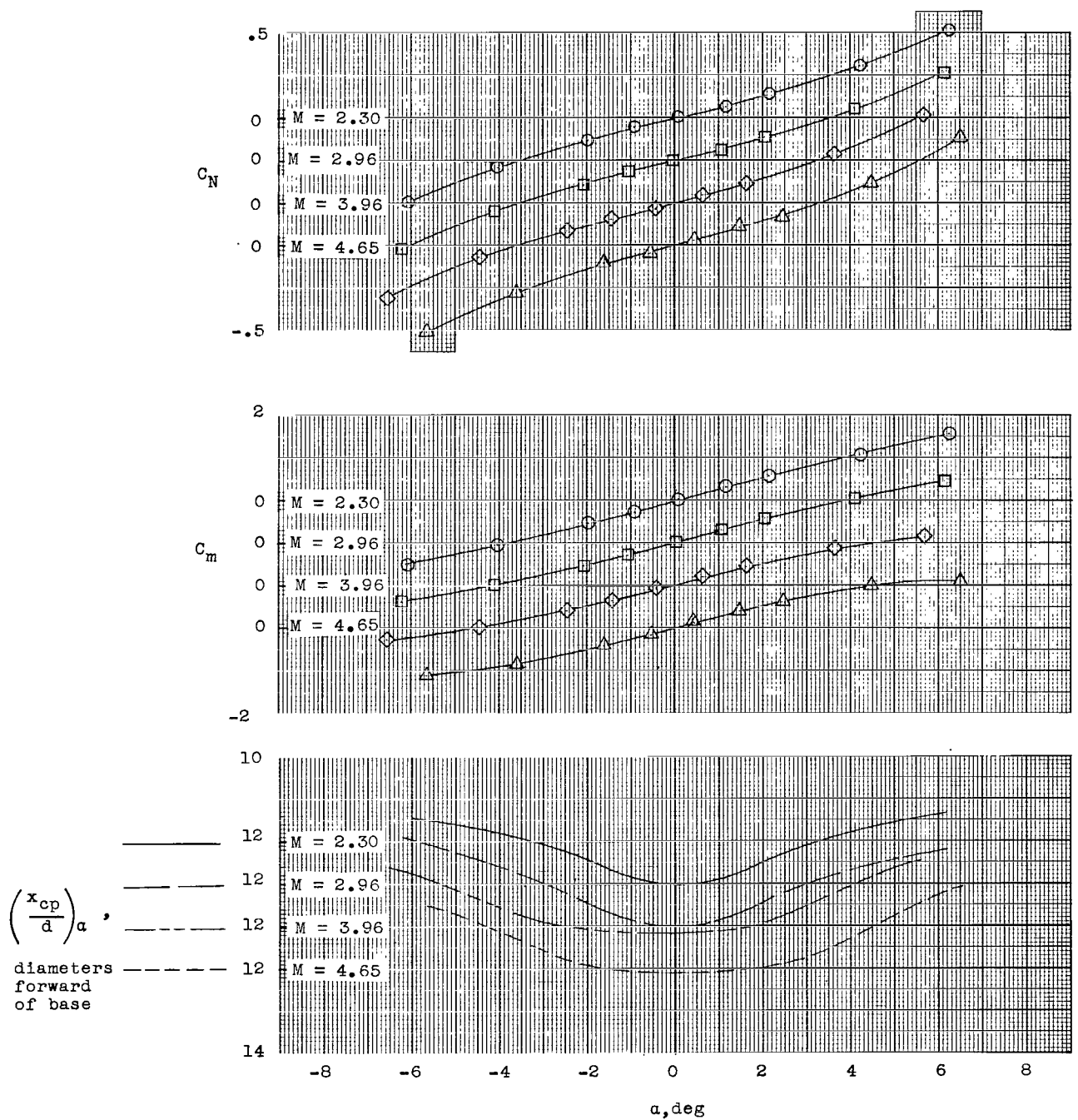
(b) C_m of basic configuration and effect of control-rocket fairings and auxiliary rockets.
 $\beta \approx 0^\circ$.

Figure 6.- Continued.



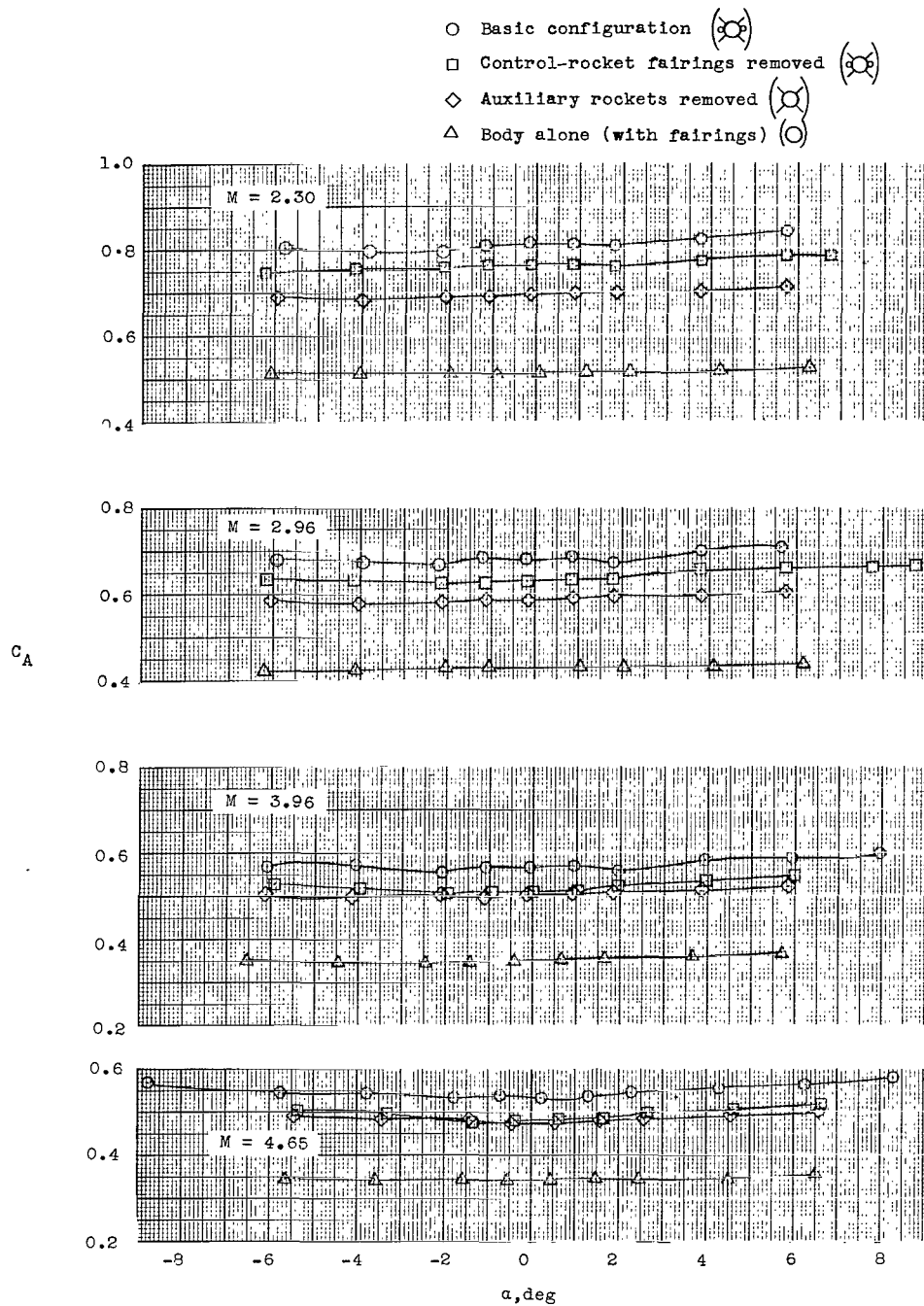
(c) $\left(\frac{x_{cp}}{d}\right)_\alpha$ of basic configuration and effect of control-rocket fairings and auxiliary rockets.
 $\beta \approx 0^\circ$.

Figure 6.- Continued.



(d) C_N , C_m , and $\left(\frac{x_{cp}}{d}\right)_\alpha$ of body-alone configuration (with fairings). $\beta \approx 0^\circ$.

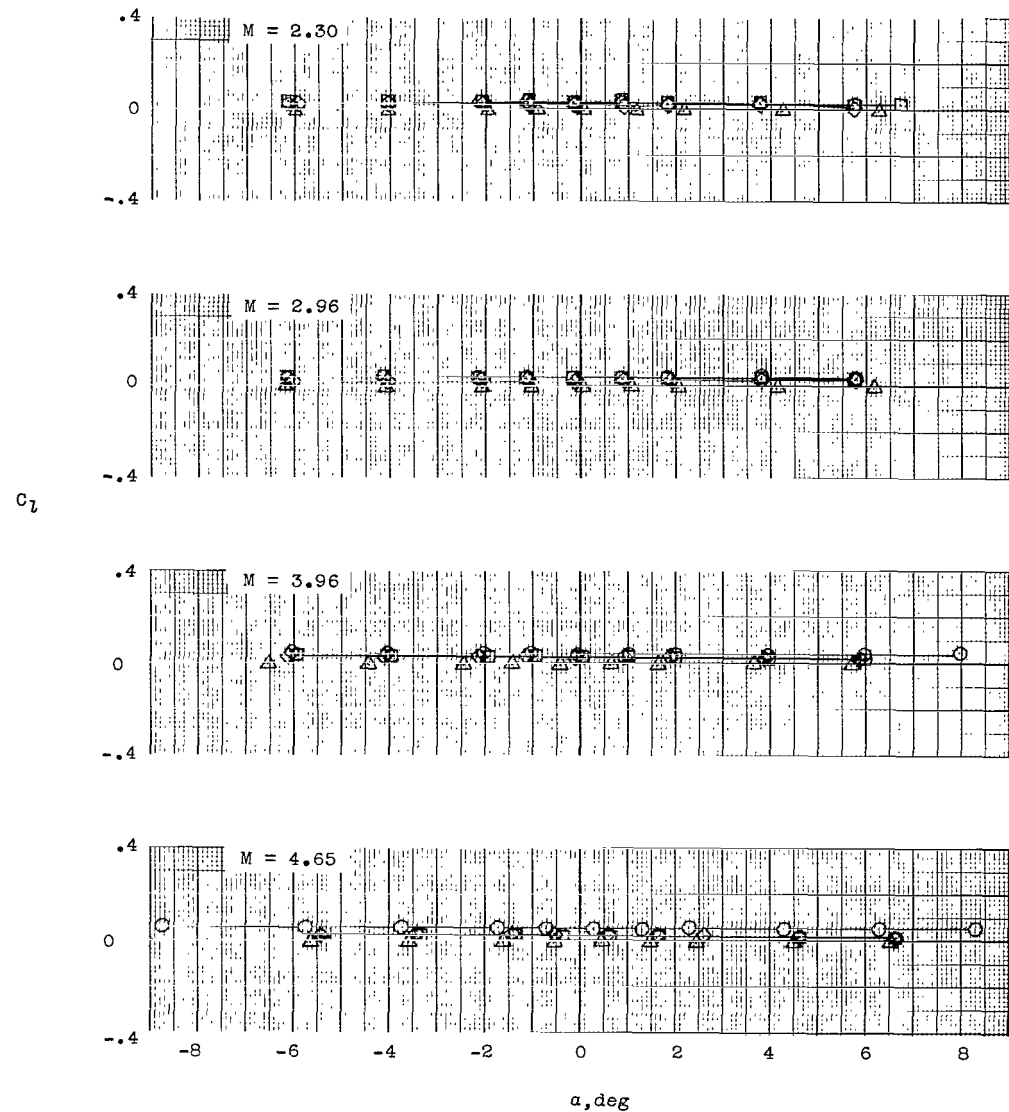
Figure 6.- Continued.



(e) C_A of basic configuration with effect of control-rocket fairings, auxiliary rockets, and C_A of body alone (with fairings). $\beta \approx 0^\circ$.

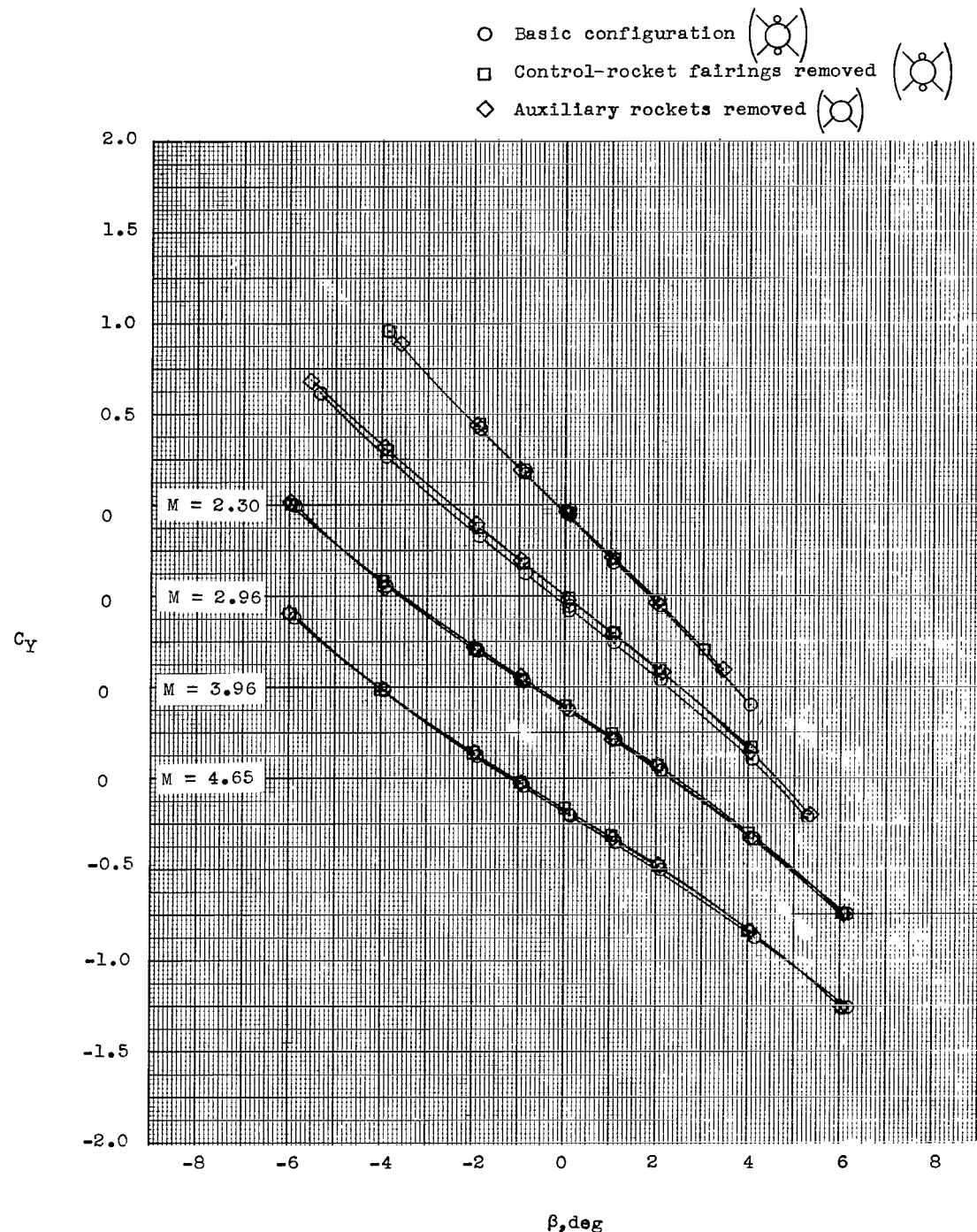
Figure 6.- Continued.

○ Basic configuration (○)
 □ Control-rocket fairings removed (○)
 ◇ Auxiliary rockets removed (○)
 △ Body alone (with fairings) (○)



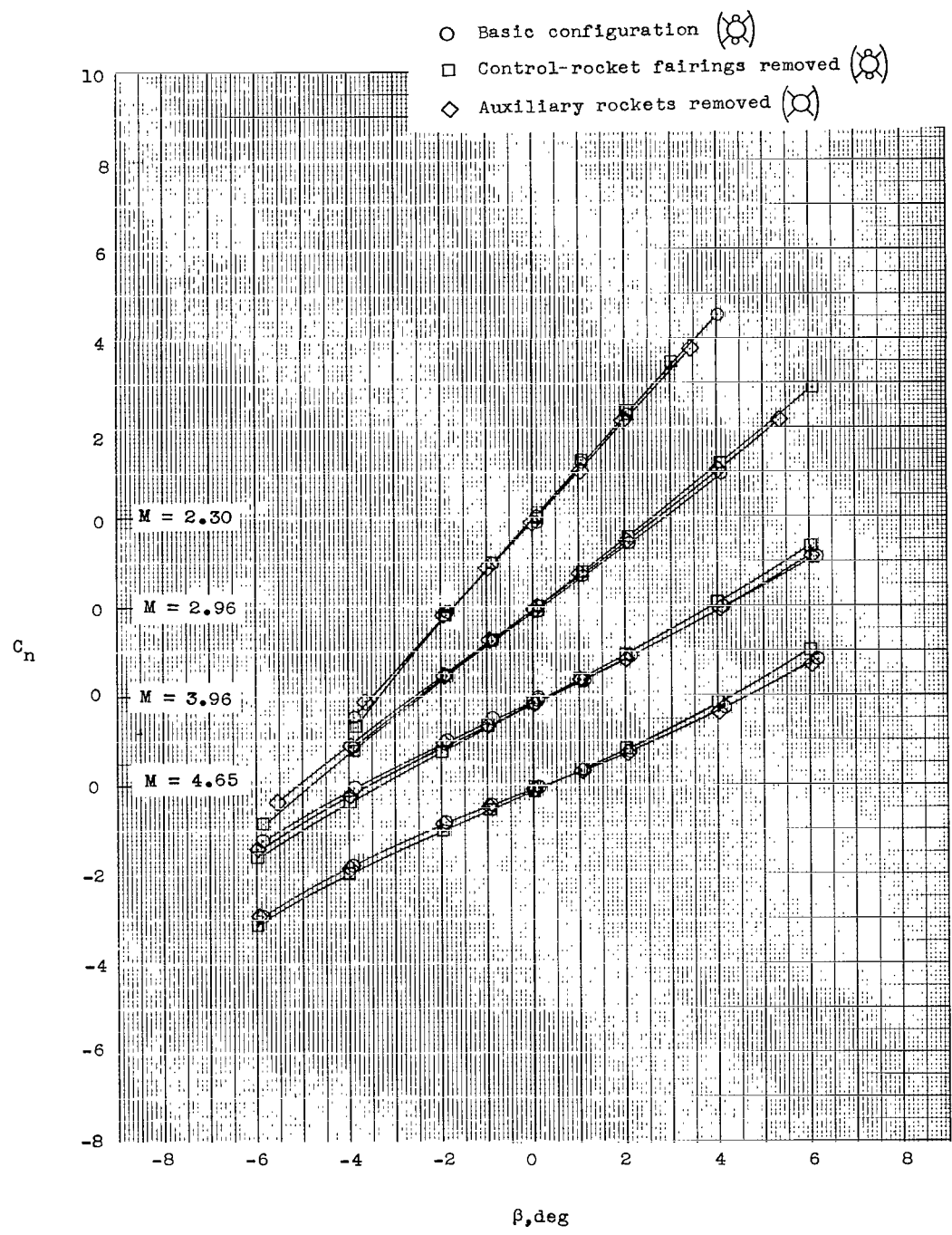
(f) C_l of basic configuration with effect of control-rocket fairings, auxiliary rockets, and C_l of body alone (with fairings). $\beta \approx 0^\circ$.

Figure 6.- Continued.



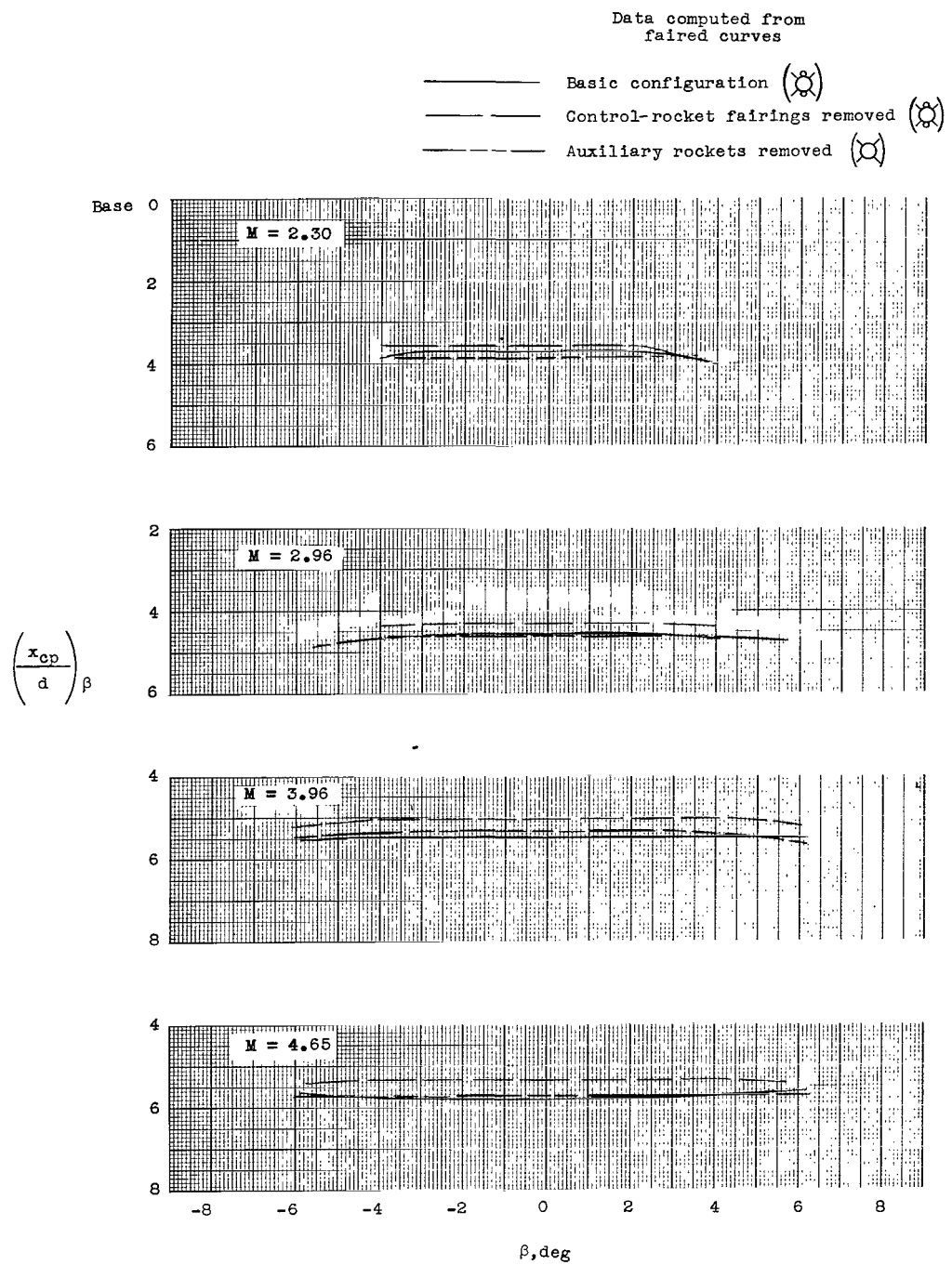
(g) C_Y of basic configuration with effect of control-rocket fairings and auxiliary rockets. $\alpha = 0^\circ$.

Figure 6.- Continued.



(h) C_n of basic configuration and effect of control-rocket fairings and auxiliary rockets.
 $\alpha \approx 0^\circ$.

Figure 6.- Continued.



(i) $\left(\frac{x_{cp}}{d}\right)_{\beta}$ of basic configuration and effect of control-rocket fairings and auxiliary rockets.
 $\alpha \approx 0^\circ$.

Figure 6.- Continued.

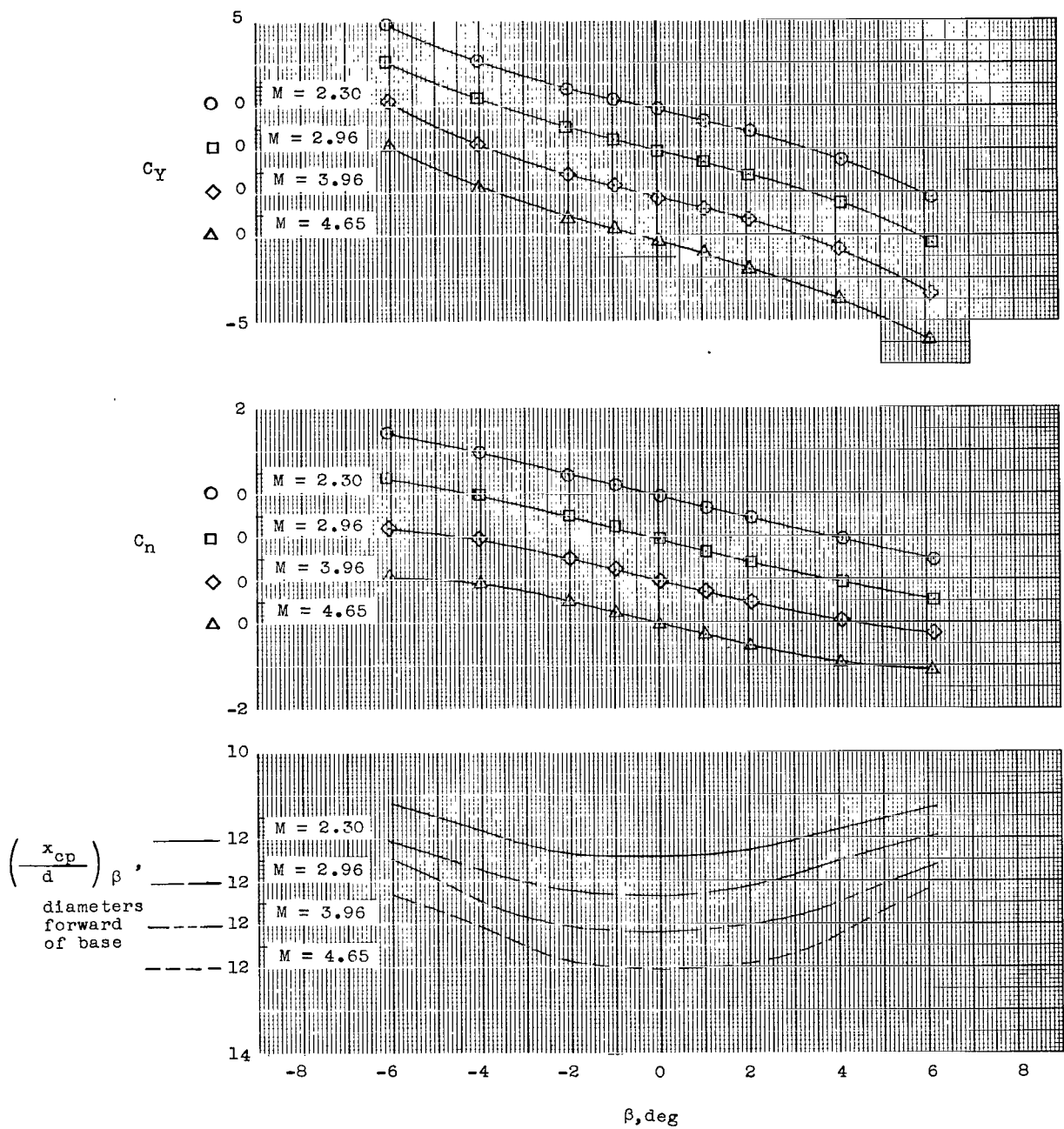
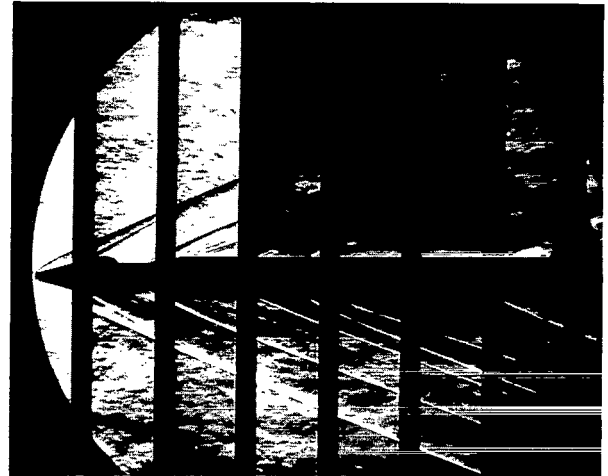


Figure 6.- Continued.



$\alpha \approx 0^\circ$; $M = 2.30$



$\alpha \approx 0^\circ$; $M = 2.96$



$\alpha \approx 0^\circ$; $M = 3.96$

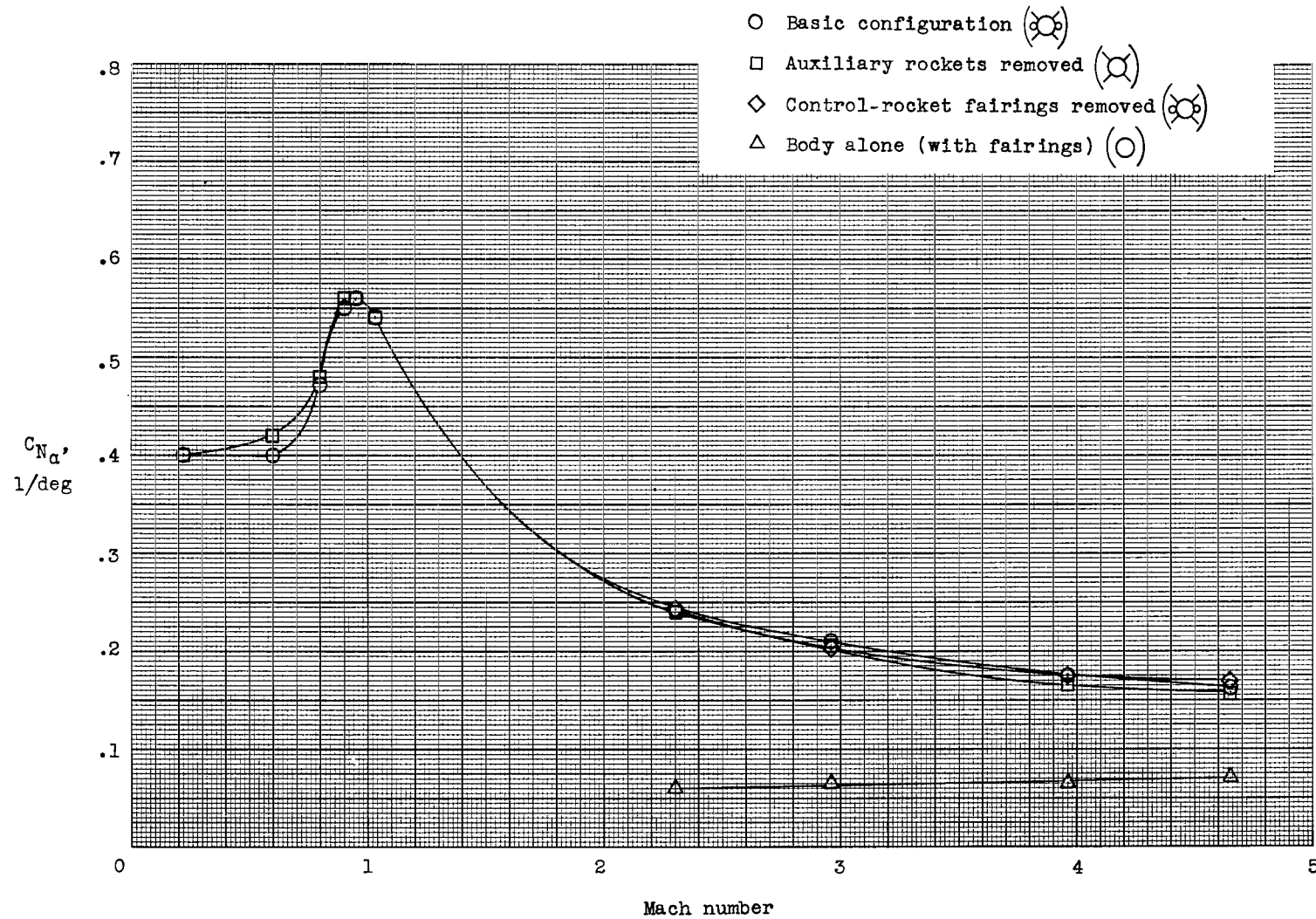


$\alpha \approx 0^\circ$; $M = 4.65$

(k) Schlieren photographs of supersonic flow over complete model.

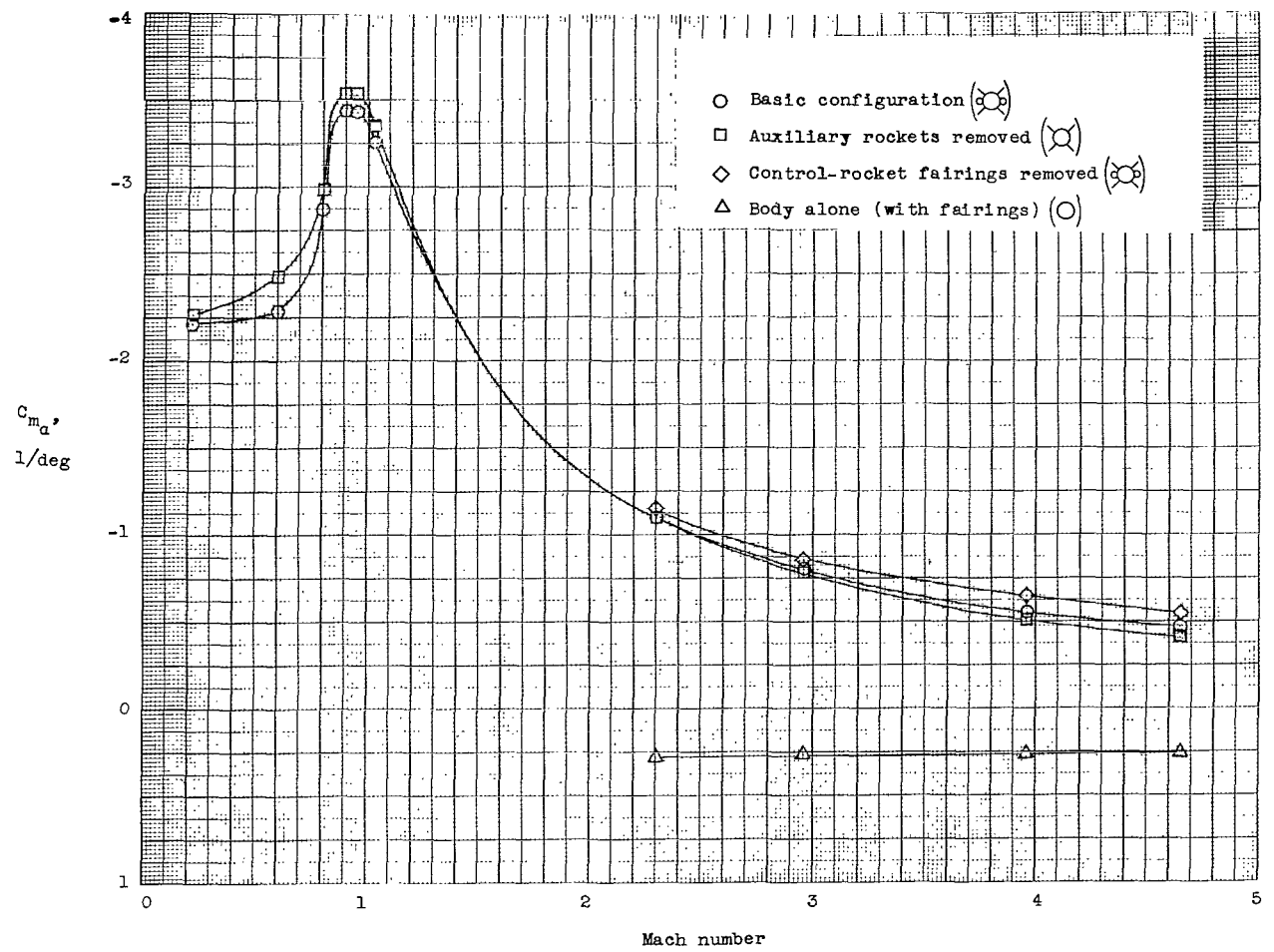
L-64-4752

Figure 6.- Concluded.



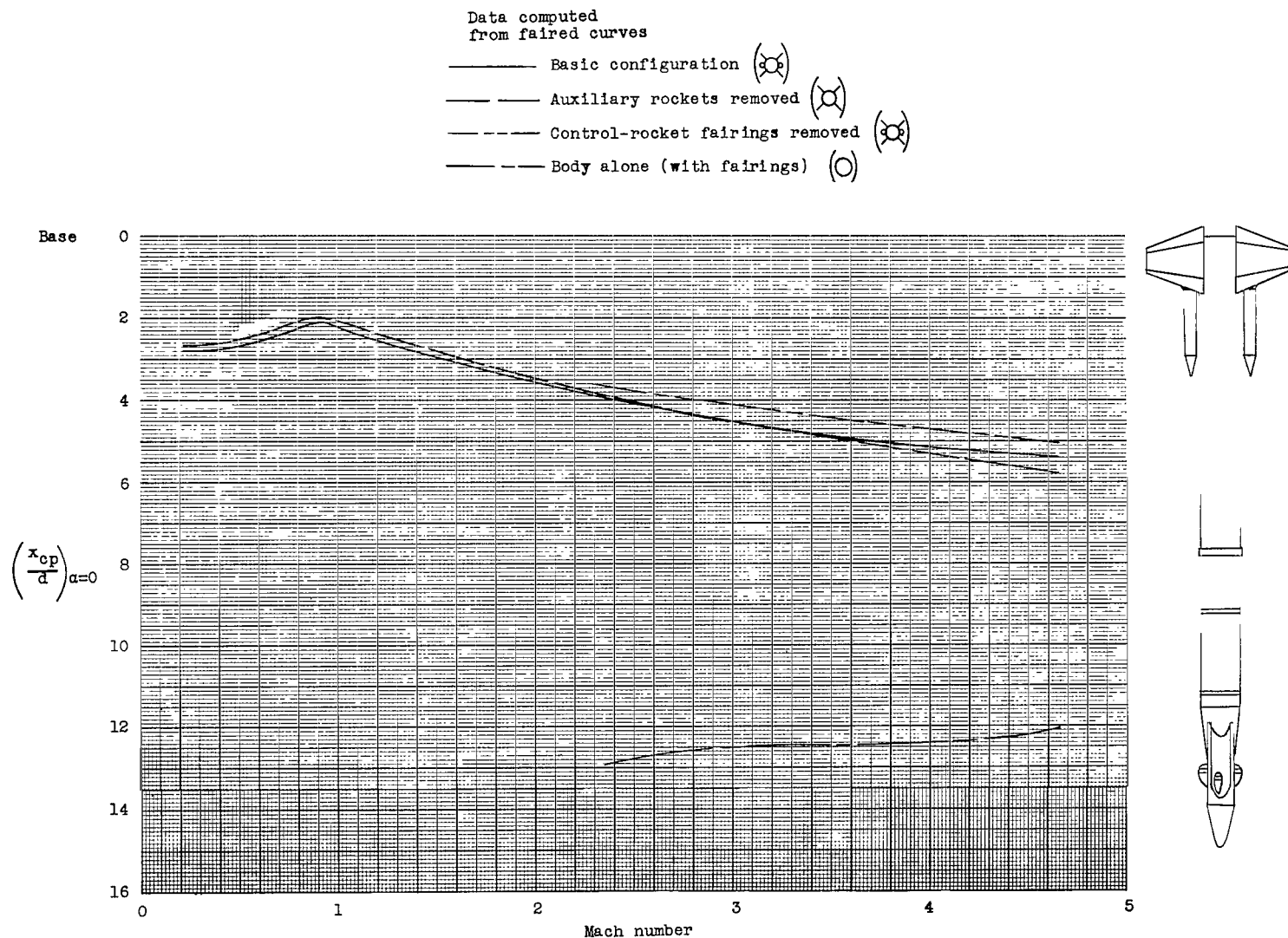
(a) $C_{N\alpha}'$

Figure 7.- Effect of Mach number, auxiliary rockets, and control-rocket fairings on zero angle of attack and sideslip characteristics of basic configuration. Characteristics of body alone are also shown.



(b) C_{m_a} .

Figure 7.- Continued.



$$(c) \quad \left(\frac{x_{cp}}{d}\right)_{\alpha=0}.$$

Figure 7.- Continued.

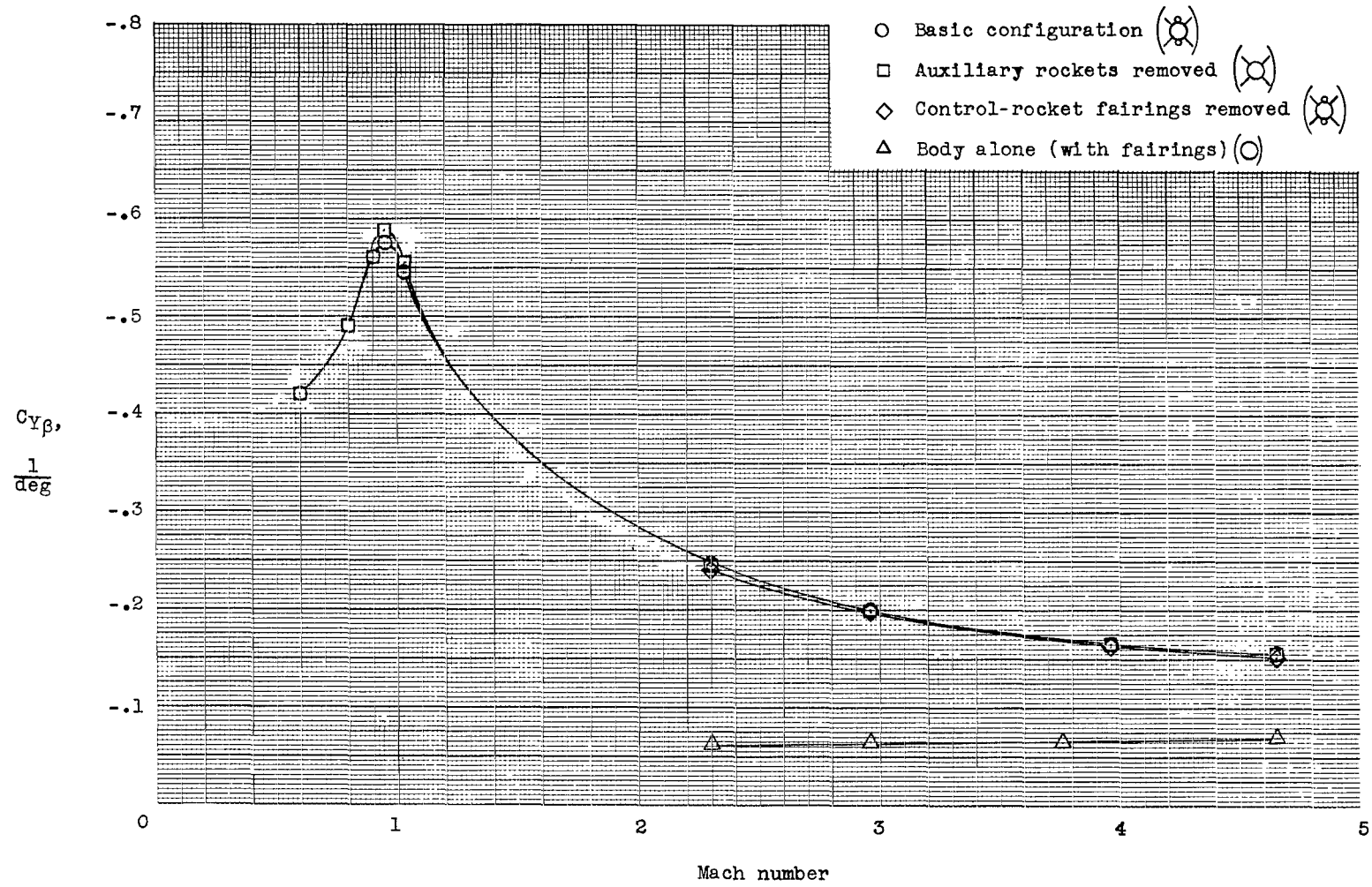
(d) $C_{Y\beta}$.

Figure 7.- Continued.

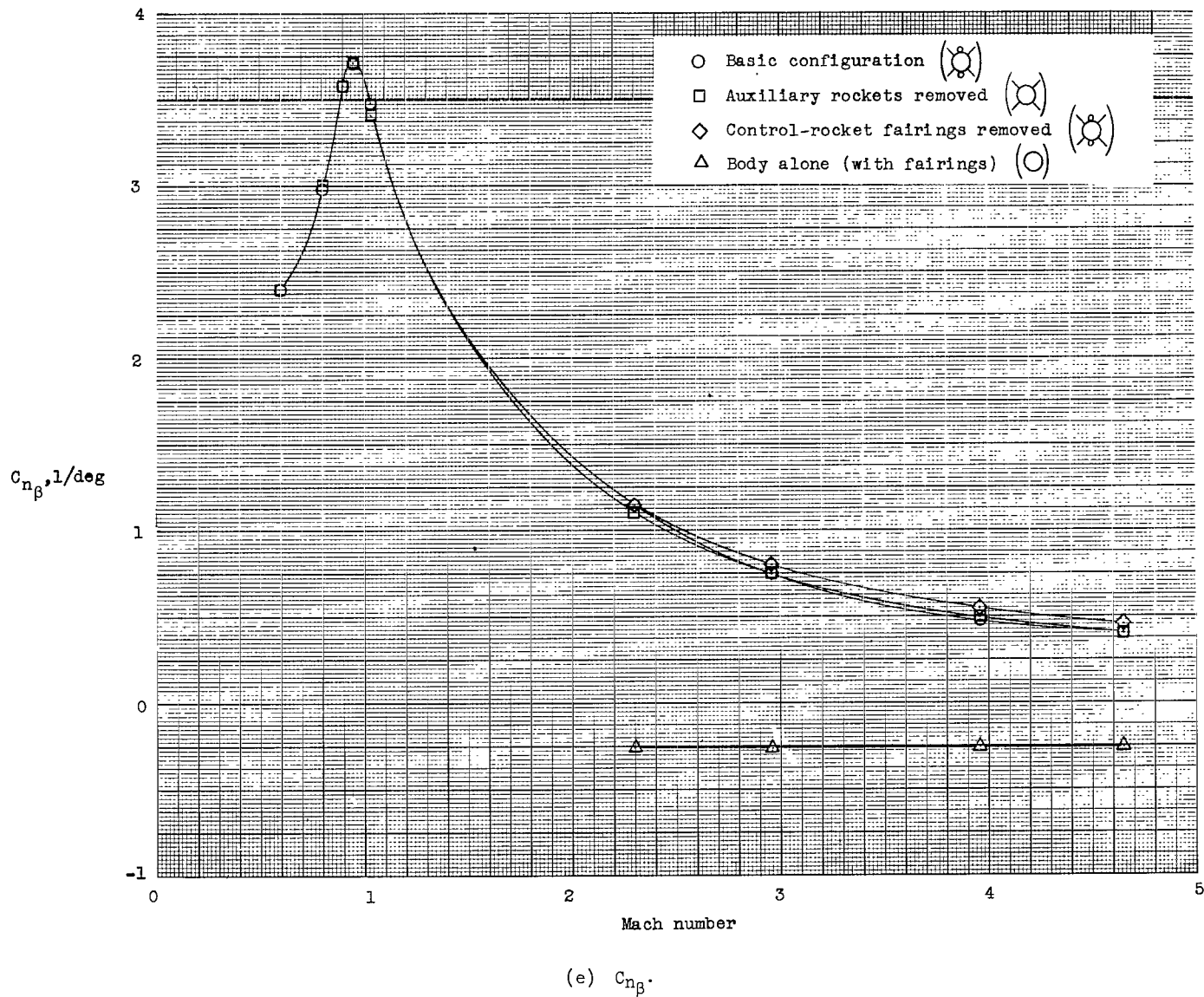


Figure 7.- Continued.

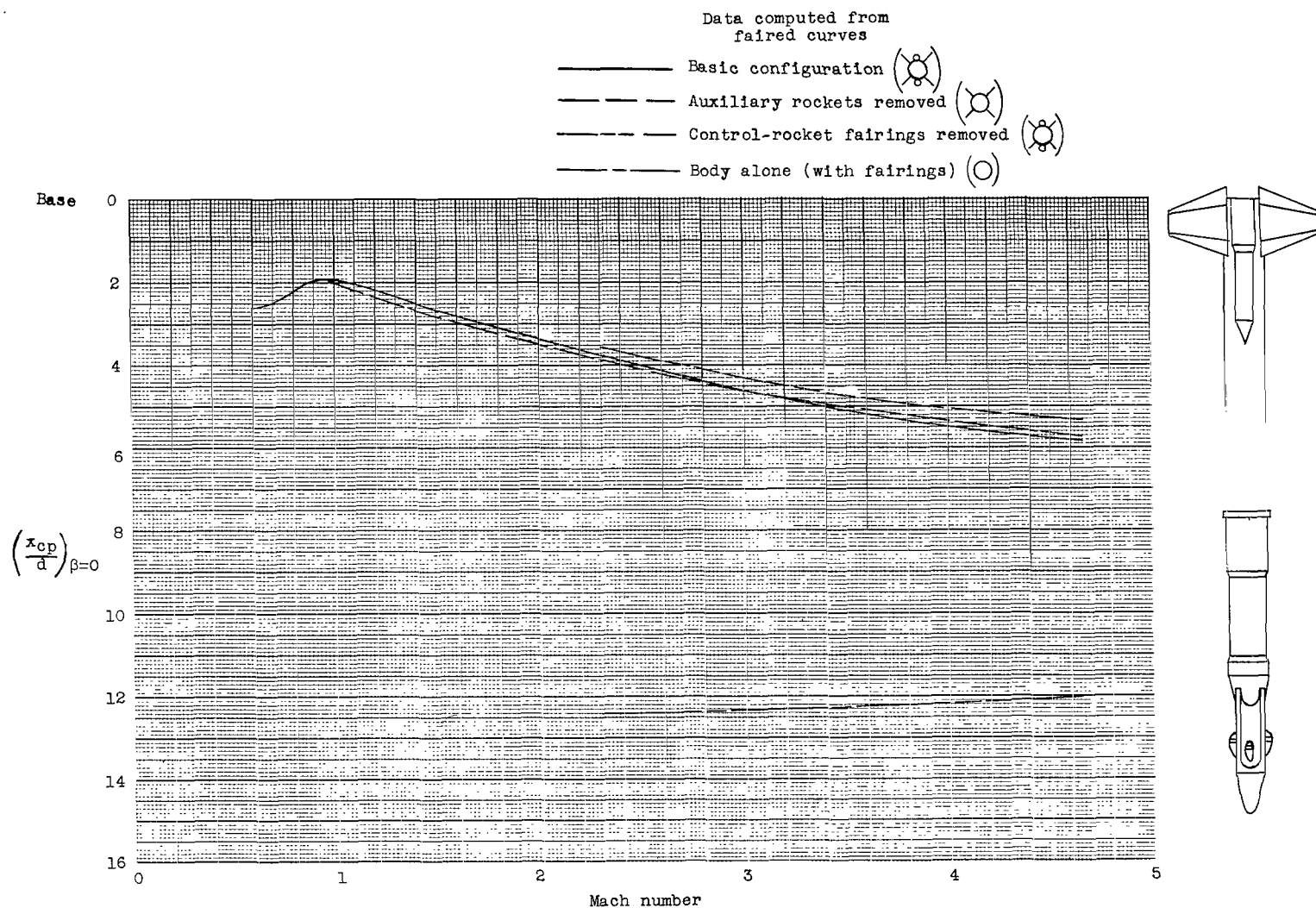
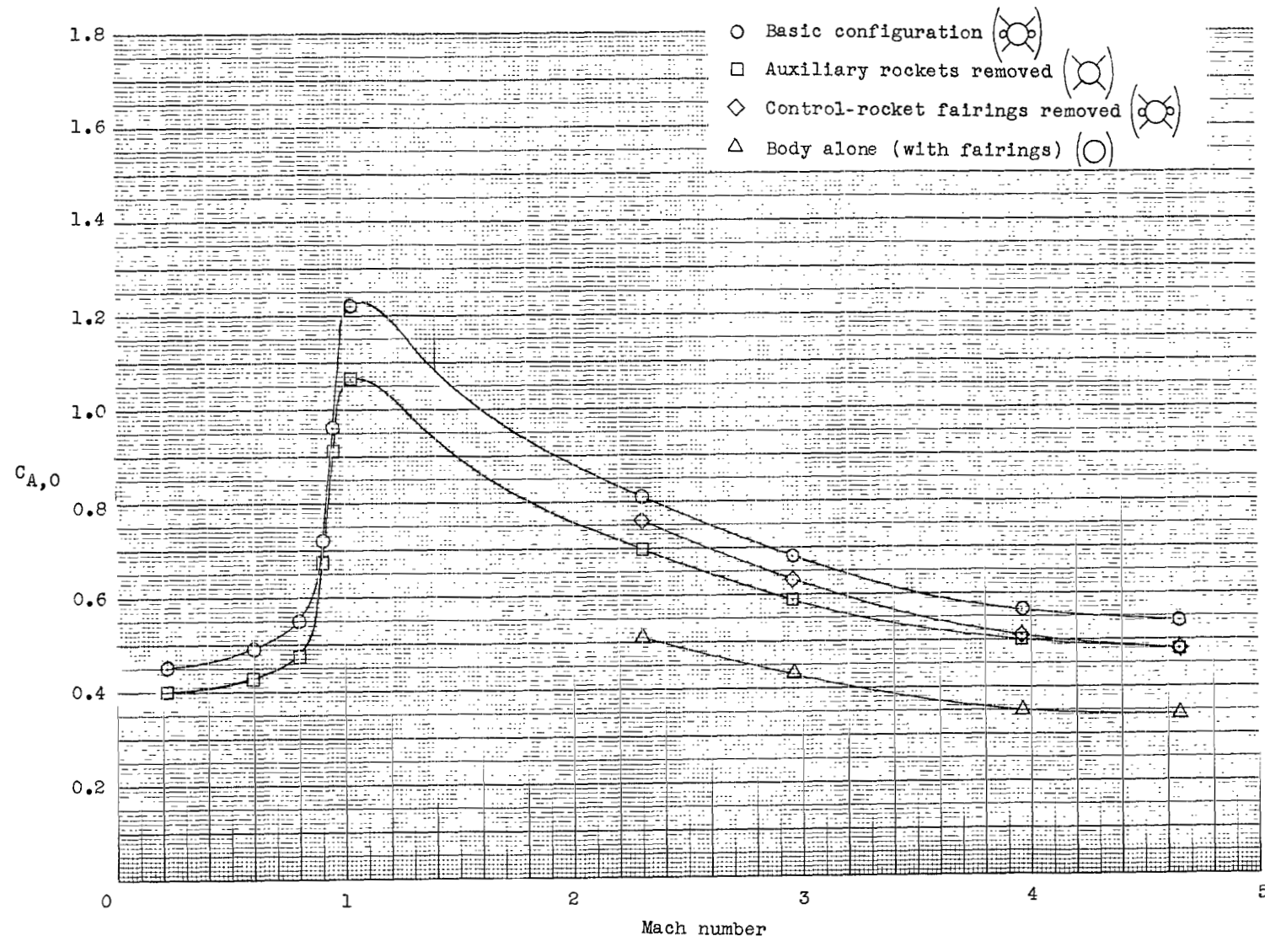
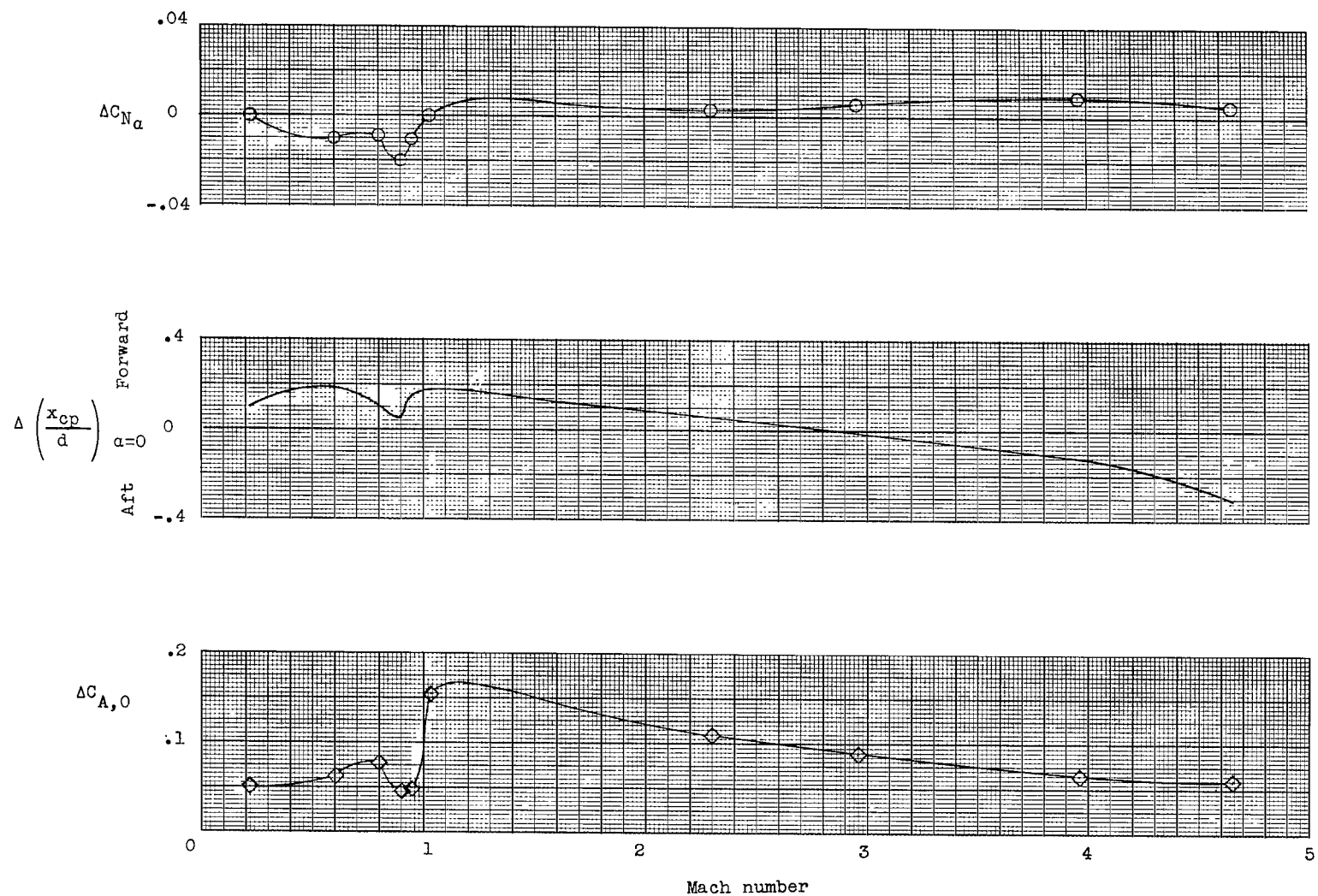


Figure 7.- Continued.



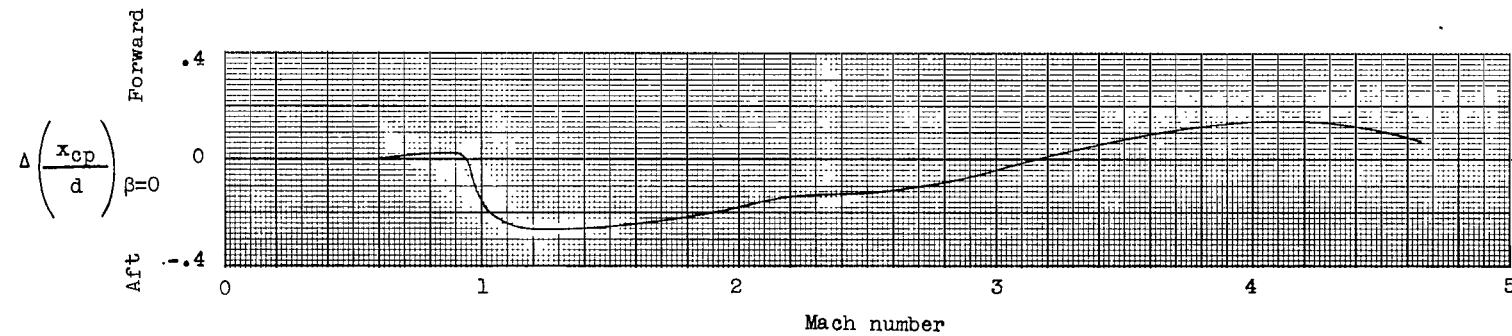
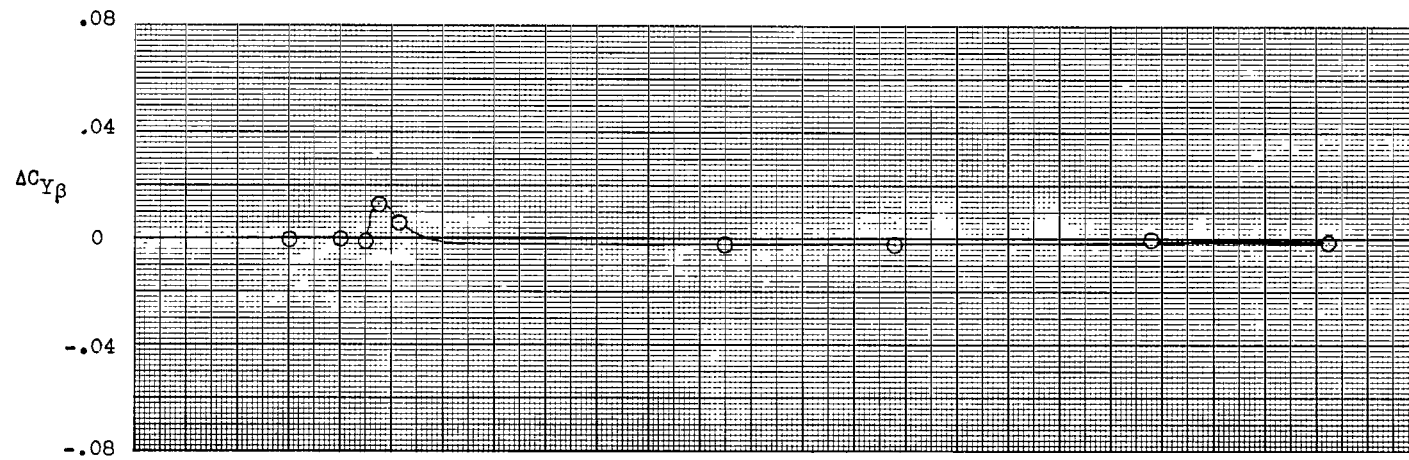
(g) $C_{A,0}$.

Figure 7.- Continued.



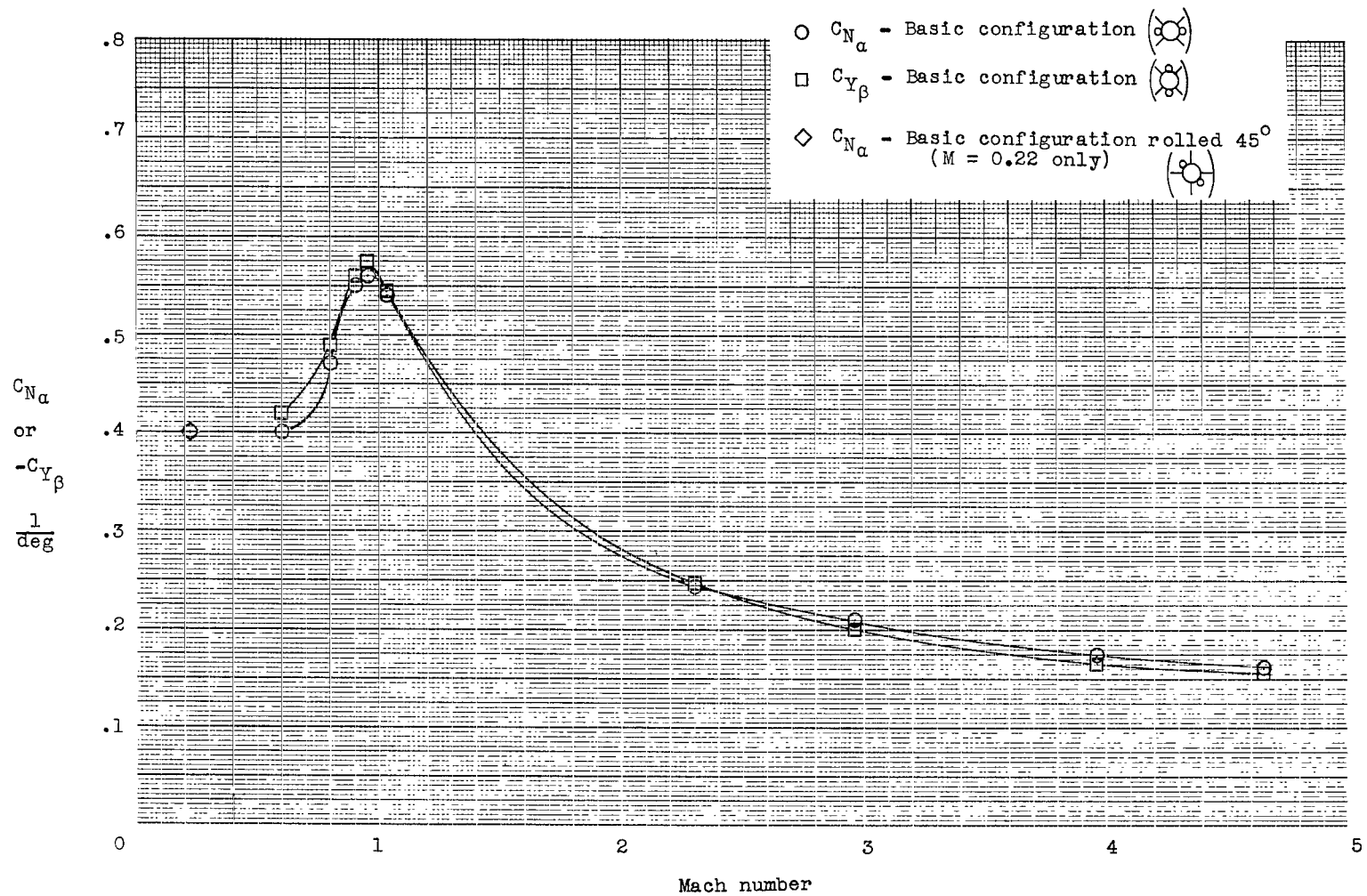
(h) $\Delta C_{N\alpha}$, $\Delta \left(\frac{x_{cp}}{d} \right)_{\alpha=0^\circ}$, $\Delta C_{A,0}$ due to adding auxiliary rockets to fin-body combination.

Figure 7.- Continued.



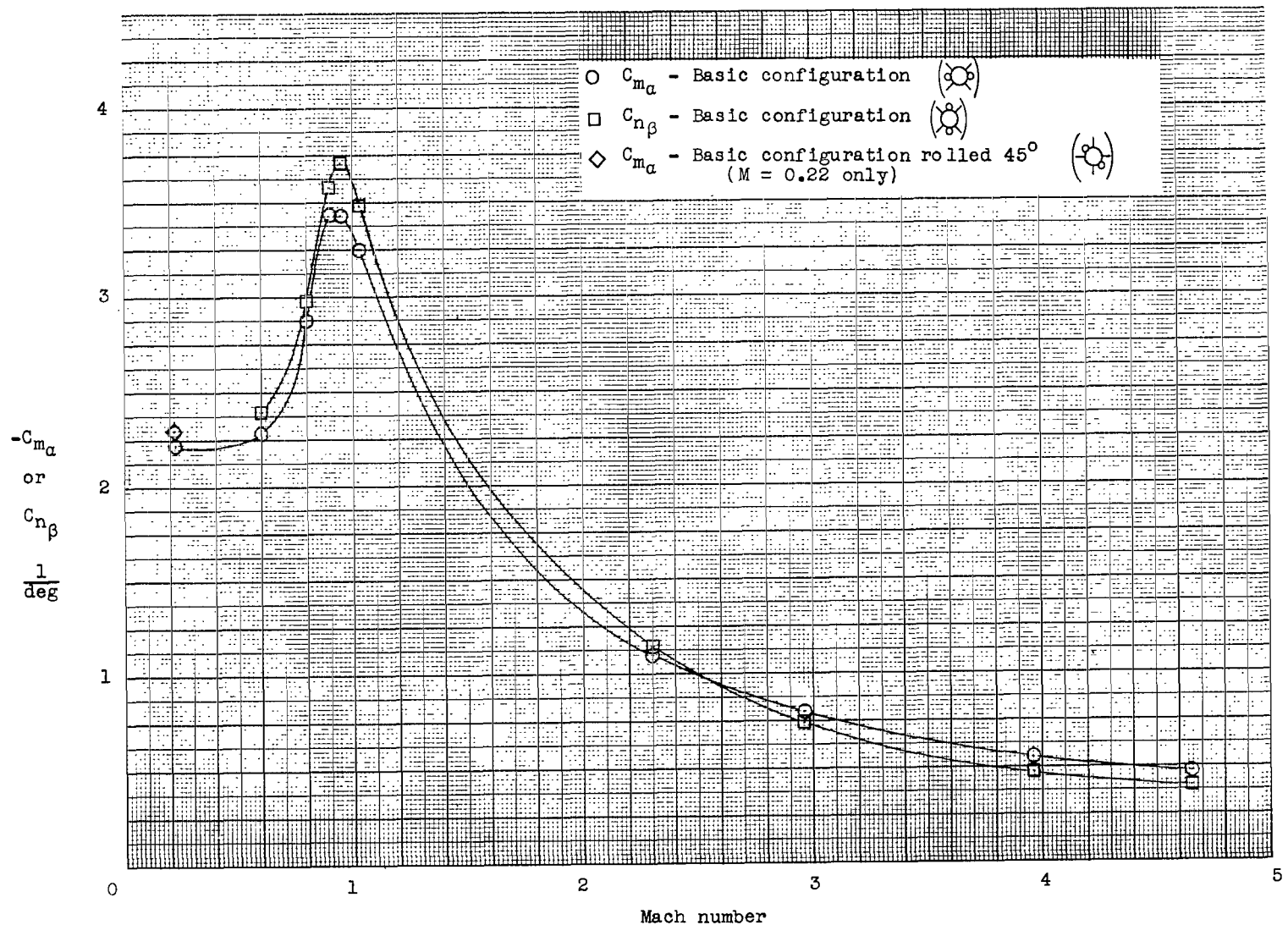
(i) $\Delta C_{Y\beta}$ and $\Delta \left(\frac{x_{cp}}{d} \right)_{\beta=0}$ due to adding auxiliary rockets to fin-body combination.

Figure 7.- Concluded.



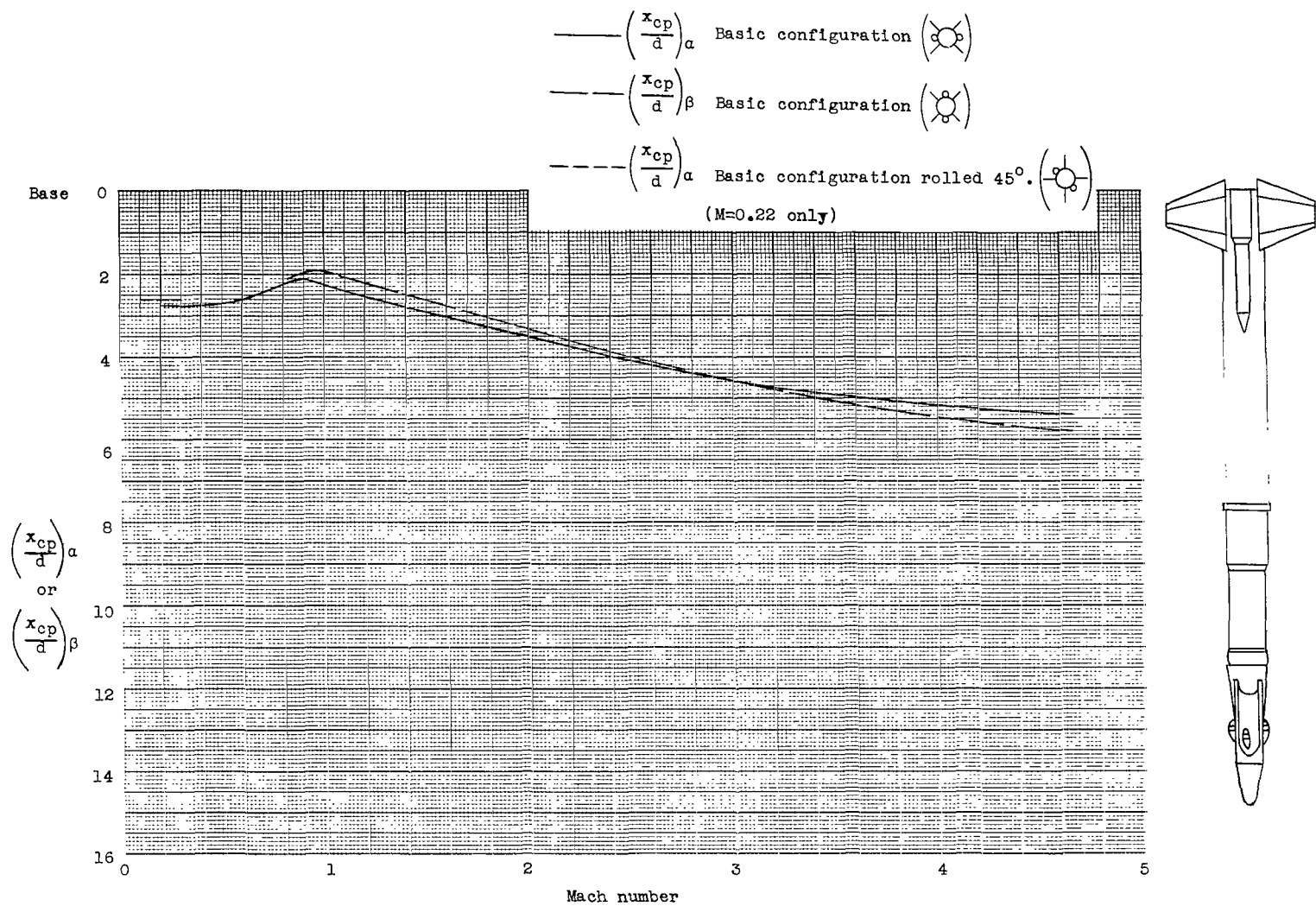
(a) Force derivative.

Figure 8.- Effect of configuration asymmetries on aerodynamic characteristics of basic configuration.



(b) Moment derivative.

Figure 8.- Continued.



(c) Center of pressure.

Figure 8.- Concluded.

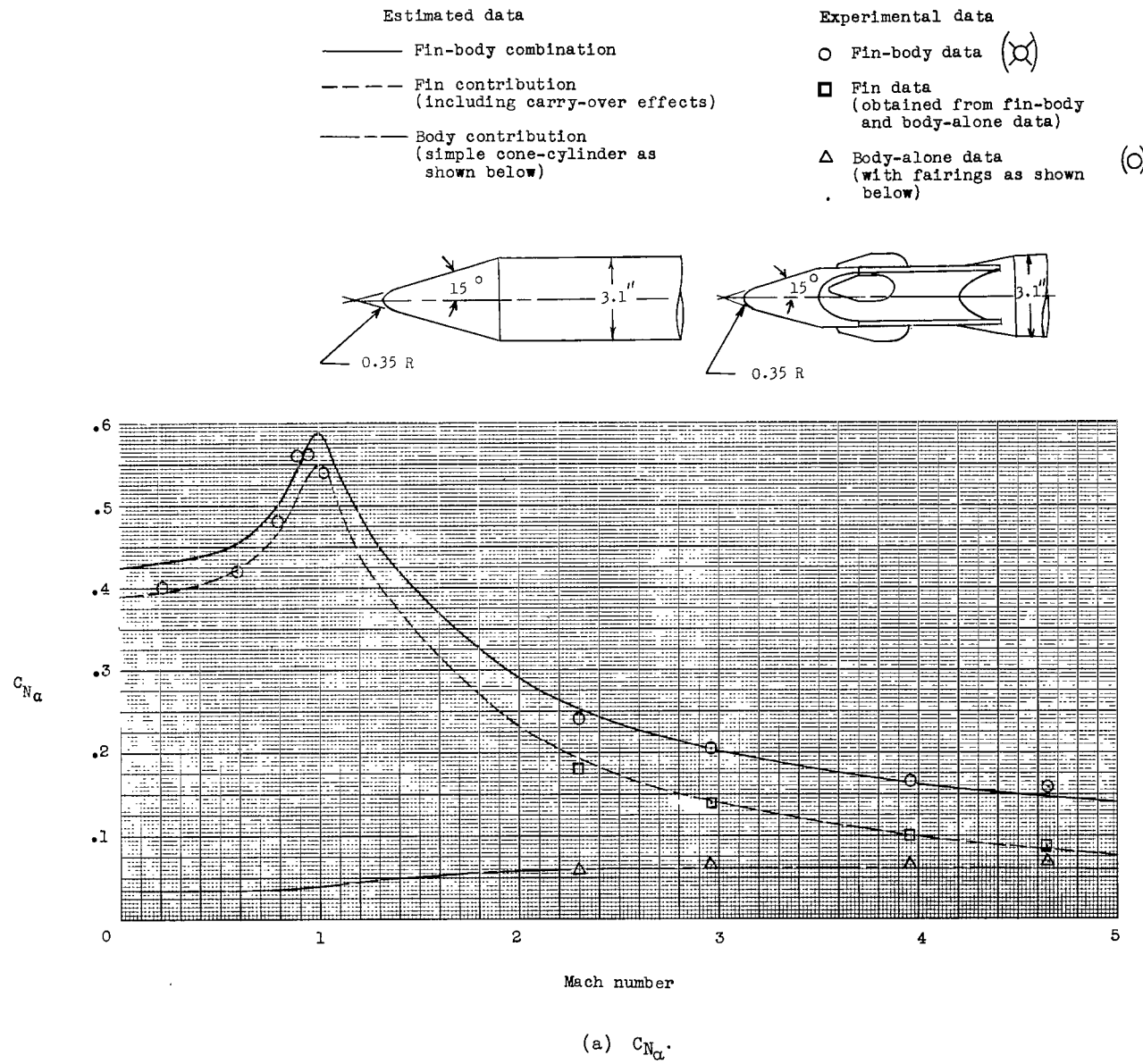


Figure 9.- Comparison of estimated data with measured fin and body contributions to aerodynamics.

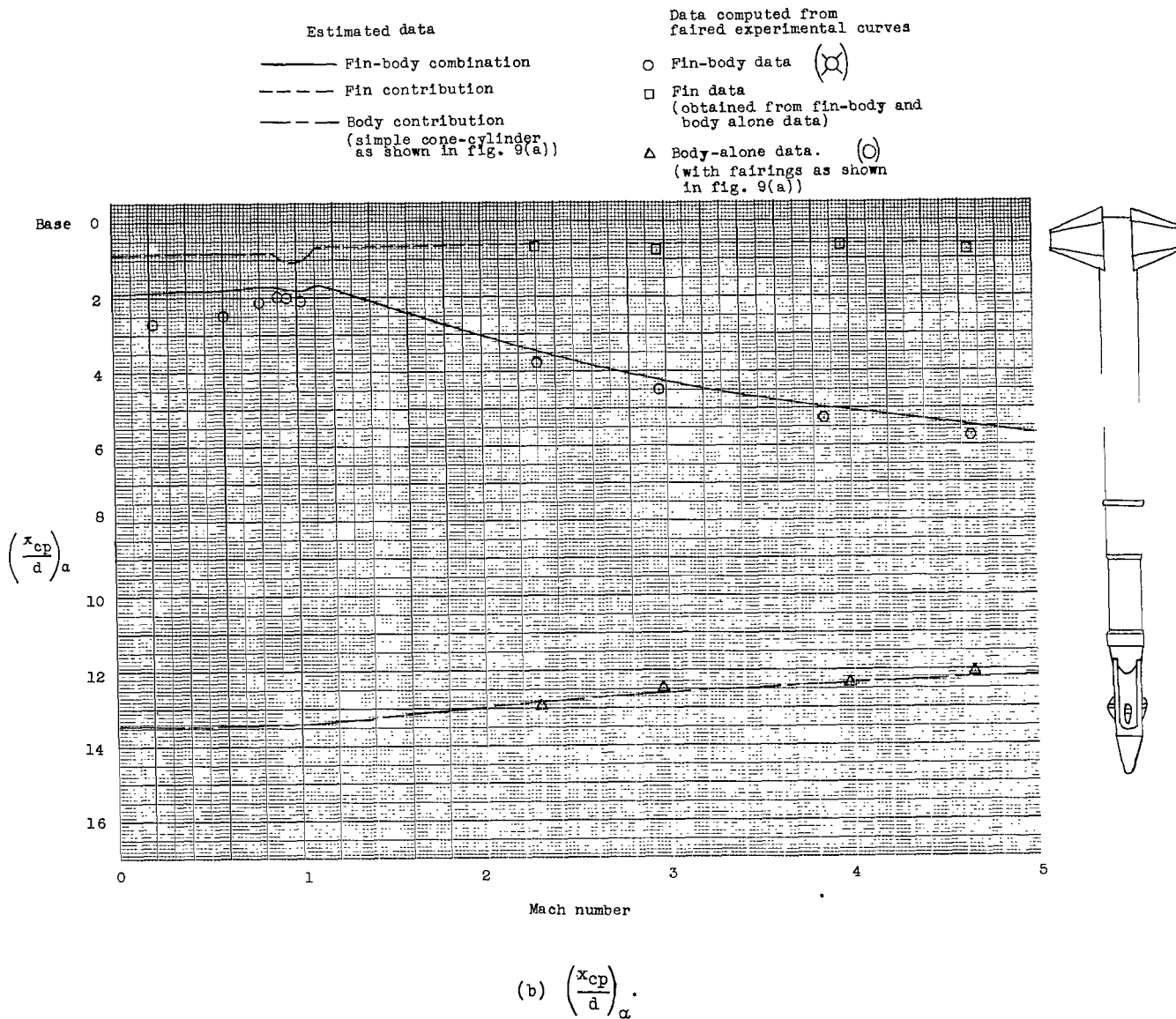
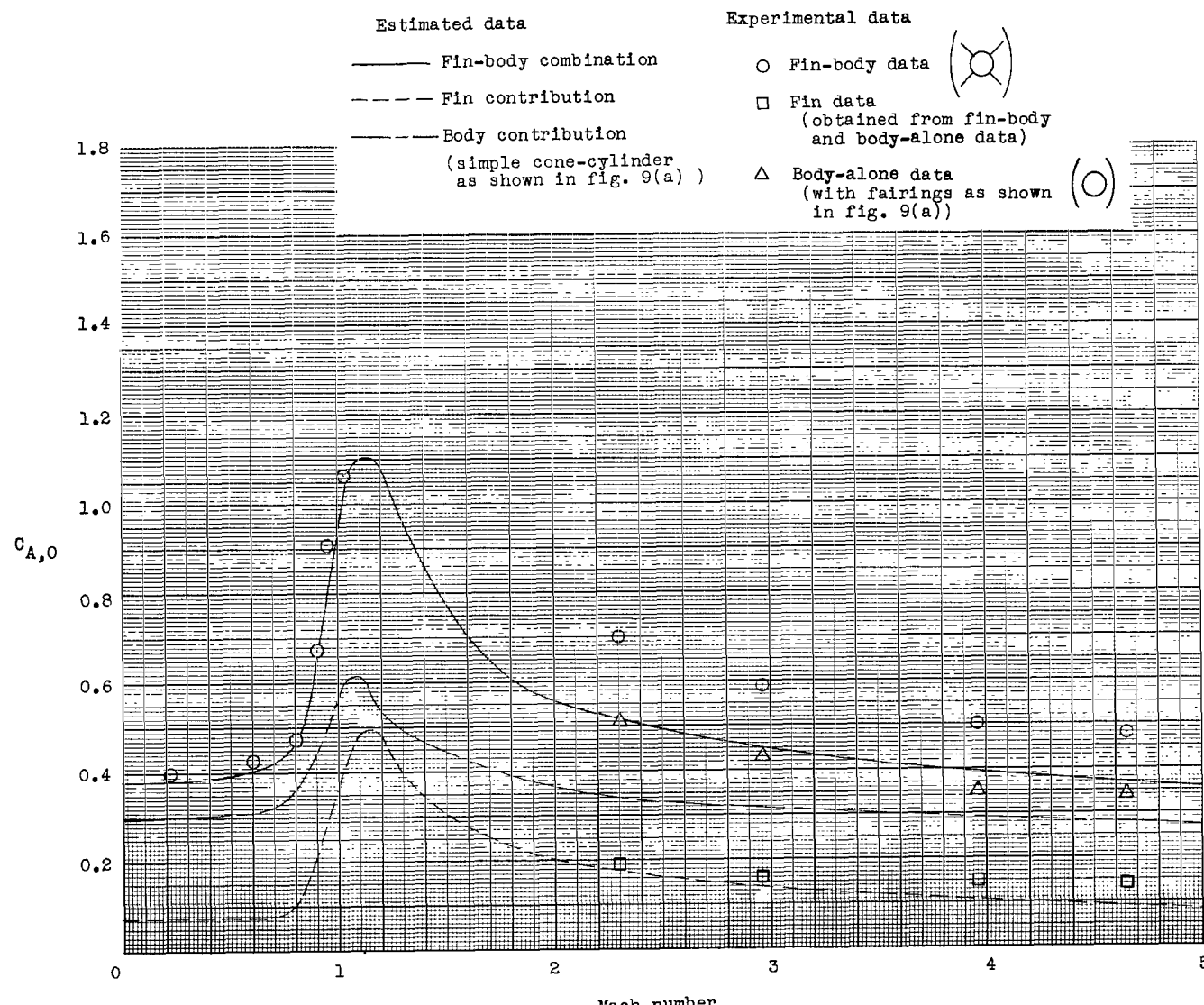


Figure 9.- Continued.



(c) $C_{A,0}$.

Figure 9.- Concluded.